Disruption of hepatic small heterodimer partner induces dissociation of steatosis and inflammation in experimental nonalcoholic steatohepatitis

Received for publication, July 17, 2019, and in revised form, November 23, 2019 Published, Papers in Press, December 12, 2019, DOI 10.1074/jbc.RA119.010233

Nancy Magee[‡], An Zou[‡], Priyanka Ghosh[‡], Forkan Ahamed[‡], Don Delker[§], and Yuxia Zhang[‡¶1]

From the [‡]Department of Pharmacology, Toxicology, and Therapeutics, University of Kansas Medical Center, Kansas City, Kansas 66160, the [§]Department of Medicine, University of Utah School of Medicine, Salt Lake City, Utah 84108, and the [¶]Liver Center, University of Kansas Medical Center, Kansas City, Kansas 66160

Edited by Dennis R. Voelker

Nonalcoholic steatohepatitis (NASH) is a leading cause of chronic liver disease worldwide and is characterized by steatosis, inflammation, and fibrosis. The molecular mechanisms underlying NASH development remain obscure. The nuclear receptor small heterodimer partner (*Shp*) plays a complex role in lipid metabolism and inflammation. Here, we sought to determine SHP's role in regulating steatosis and inflammation in NASH. *Shp* deletion in murine hepatocytes ($Shp^{Hep-/-}$) resulted in massive infiltration of macrophages and $CD4^+$ T cells in the liver. $Shp^{Hep-/-}$ mice developed reduced steatosis, but surprisingly increased hepatic inflammation and fibrosis after being fed a high-fat, -cholesterol, and -fructose (HFCF) diet. RNA-Seq analysis revealed that pathways involved in inflammation and fibrosis are significantly activated in the liver of $Shp^{Hep-/-}$ mice fed a chow diet. After having been fed the HFCF diet, WT mice displayed up-regulated peroxisome proliferator-activated receptor γ (*Pparg*) signaling in the liver; however, this response was completely abolished in the $Shp^{Hep-/-}$ mice. In contrast, livers of $Shp^{Hep-/-}$ mice had consistent NF-κB activation. To further characterize the role of *Shp* specifically in the transition of steatosis to NASH, mice were fed the HFCF diet for 4 weeks, followed by *Shp* deletion. Surprisingly, *Shp* deletion after steatosis development exacerbated hepatic inflammation and fibrosis without affecting liver steatosis. Together, our results indicate that, depending on NASH stage, hepatic *Shp* plays an opposing role in steatosis and inflammation. Mechanistically, *Shp* deletion in hepatocytes activated NF-κB and impaired *Pparg* activation, leading to the dissociation of steatosis, inflammation, and fibrosis in NASH development.

This work was supported by National Institutes of Health Grants R01DK119131, K22CA184146, P20GM103549, P30GM118247, P20GM-103418, T32ES007079, and UL1 TR002366; a KUMC Enhancement Award; an American Association for the Study of Liver Diseases (AASLD) Bridging Award; and American Cancer Society (ACS) Institutional Research Grant (IRG) 16-194-07. The authors declare that they have no conflicts of interest with the contents of this article. The content is solely the responsibility of the authors and does not necessarily represent the official views of the National Institutes of Health.

This article contains supporting information.

The RNA-Seq data have been deposited in the GEO database under the accession number GSE133566.

[1] To whom correspondence should be addressed: Dept. of Pharmacology, Toxicology and Therapeutics, University of Kansas Medical Center, Kansas City, KS 66160. Tel.: 913-588-1749; E-mail: lzhang5@kumc.edu.

Nonalcoholic fatty liver disease (NAFLD)[2] is rapidly becoming a major health concern worldwide due to the epidemic of obesity and diabetes (1). Whereas simple steatosis is generally considered a relatively benign condition, ~20–30% of these patients will develop nonalcoholic steatohepatitis (NASH), a more serious condition characterized by steatosis with hepatocyte injury, liver inflammation, and fibrosis, which can further progress to irreversible cirrhosis and hepatocellular carcinoma with no effective therapies (2–4). Despite the increasing prevalence of NASH and its burden to the healthcare system, the molecular mechanisms underlying NASH development still remain obscure, leading to a lack of mechanism-based targeted treatment options for NASH. Thus, understanding the molecular machinery that causes NASH will provide new insights into developing effective prevention and therapeutic strategies for this unresolved disease.

Small heterodimer partner (*Nr0b2*, *Homo sapiens SHP*; *Mus musculus Shp*) is an atypical nuclear receptor due to its lack of a DNA-binding domain (5). As an orphan nuclear receptor without a known ligand, SHP represses bile acid synthesis (6, 7), controls energy metabolism (8), and regulates glucose homeostasis (9, 10) via direct interactions with numerous nuclear receptors and transcription factors (11). In support of its important role in metabolic diseases, mutations in the *Shp* gene have been correlated with obesity and susceptibility to type 2 diabetes (12).

SHP is involved in lipid metabolism. Earlier studies demonstrate that hepatic SHP overexpression increases liver lipid levels (13). Consistently, *Shp*-deficient mice are protected from high-fat diet–induced hepatic steatosis (14, 15). These studies indicate that antagonizing SHP may be beneficial to treat liver steatosis. In contrast, a recent study reported that *Shp* was not suppressed in the steatotic livers but was decreased in NASH livers, such as tetracycline-treated livers, methionine choline-deficient diet–induced NASH livers, and glycine *N*-methyl-

[2] The abbreviations used are: NAFLD, nonalcoholic fatty liver disease; NASH, nonalcoholic steatohepatitis; SHP, small heterodimer partner; DAMP, damage-associated molecular pattern molecule; ALT, alanine aminotransferase; TUNEL, terminal deoxynucleotidyl transferase dUTP nick-end labeling; DEG, differentially expressed gene; GO, gene ontology; PPAR, peroxisome proliferator-activated receptor; H&E, hematoxylin and eosin; HSC, hepatic stellate cell; FFA, free fatty acid; BA, bile acid; KEGG, Kyoto Encyclopedia of Genes and Genomes; qPCR, quantitative PCR; OD, optical density.

transferase-deficient ($Gnmt^{-/-}$) mouse livers (16). Similarly, our recent study also found that SHP was markedly decreased in the livers of patients with NASH and in diet-induced mouse NASH (17). Additionally, hepatic SHP overexpression after steatosis development dramatically prevented steatosis progression to NASH by attenuating liver inflammation and fibrosis (17). These results indicate that the role of SHP in NAFLD development is complicated and could be multilayered.

A diet containing high fat, cholesterol, and fructose (HFCF; 40 kcal% fat, 2% cholesterol, 20 kcal% fructose) has been utilized to induce NASH in mice (18, 19). In this diet, excess fat induces the development of steatosis, whereas the addition of fructose and cholesterol increases hepatic damage, predisposing animals to inflammation and fibrogenesis (20). Therefore, this dietary model replicates many of the biochemical and histopathological hallmarks of clinical NAFLD progression from steatosis to NASH (17). In the current study, we fed mice an HFCF diet to dissect the role of SHP in steatosis and inflammation during NASH development.

Hepatic macrophage activation is a hallmark of NASH and is correlated with disease progression by producing proinflammatory and profibrogenic mediators (21). Although the mechanism underlying macrophage activation in NASH is incompletely understood, numerous studies demonstrate that lipotoxicity-induced hepatocyte damage triggers the release of damage-associated molecular pattern molecules (DAMPs) into the microenvironment, which stimulates macrophage activation (22, 23). Therefore, steatosis is generally positively correlated with liver inflammation and liver injury. Strikingly, in the current study, we revealed that hepatic *Shp* deletion ameliorated liver steatosis but aggravated macrophage activation in HFCF-fed mice. Mechanistically, we demonstrated that *Shp* disruption in hepatocytes activated NF-κB signaling and impaired peroxisome proliferator activated receptor γ (*Pparg*) activation, leading to the dissociation between steatosis and inflammation in NAFLD. Interestingly, *Shp* deletion after steatosis development accelerated hepatic inflammation and fibrosis without affecting liver steatosis. These findings indicate that, depending on NAFLD stage, SHP could play distinct roles in modulating steatosis, inflammation, and fibrosis.

Results

Hepatic Shp disruption in adult mice induces liver injury, inflammation, and fibrogenesis

To generate hepatocyte-specific *Shp* knockout ($Shp^{Hep-/-}$) mice and WT controls, we injected 2-month-old $Shp^{flox/flox}$ mice with either AAV8-Tbg-Cre or AAV8-Tbg-null control for 1 or 12 weeks (Fig. 1*A*). The use of the *Tbg* promoter ensures that AAV8 specifically targets hepatocytes (24). Hepatic *Shp* deletion specifically in adult mice achieved a model in which a direct assessment of hepatic *Shp* function in the adult livers could be made. This is an advantage over using mice with a germ line mutation in *Shp*, which could interfere with proper embryonic or neonatal development and alter adult hepatic function. This acute deletion approach also made it possible to distinguish the direct effects of *Shp* deletion from any secondary or compensatory effects.

The knockdown of *Shp* mRNA in the liver after Cre injection was confirmed by RT-PCR (Fig. 1*A*). The body weight gain, lean mass, and fat mass were comparable between $Shp^{Hep-/-}$ mice and WT controls after 1 week or 12 weeks of AAV8 injection (Fig. 1, *B* and *C*). To investigate whether ablation of hepatic *Shp* could affect glucose metabolism, we performed a glucose tolerance test (GTT). As shown in Fig. 1*D*, no difference in GTT was observed between $Shp^{Hep-/-}$ mice and WT controls, which was further confirmed by the quantification of areas under the curves (*AUC*) of GTT (Fig. 1*D*, *right*). Additionally, the fasting serum triglycerides, cholesterol, and glucose were similar between $Shp^{Hep-/-}$ mice and WT controls; however, the liver injury marker alanine aminotransferase (ALT) was significantly increased after 12 weeks of *Shp* deletion (Fig. 1*E*).

We next examined the liver. Both liver weight and liver/body weight ratios were comparable between $Shp^{Hep-/-}$ mice and WT controls after AAV8 injection (Fig. 1*F*). No obvious histological change was observed 1 week after *Shp* deletion; however, after 12 weeks, a massive infiltration of inflammatory cells occurred in the livers of $Shp^{Hep-/-}$ mice (Fig. 1*G*). Meanwhile, an increase in cell death was observed in $Shp^{Hep-/-}$ liver that was detected by terminal deoxynucleotidyl transferase dUTP nick-end labeling (TUNEL) staining (Fig. 1*H*), supporting the elevated serum ALT shown in Fig. 1*E*. Taken together, the above data indicate that hepatic *Shp* deletion induces liver injury.

Immunohistochemistry staining of inflammatory cell markers CD3, CD4, CD8, CD19, F4/80, and Ly6G/Gr1 revealed an elevation of $CD4^+$ T cells, B cells, macrophages, and neutrophils in the $Shp^{Hep-/-}$ liver, respectively (Fig. 2*A*). Meanwhile, an increase in liver fibrosis in $Shp^{Hep-/-}$ mice was detected by both Trichrome staining and liver hydroxyproline extraction (Fig. 2*B*). Consistently, *Shp* deletion led to a robust induction of genes involved in inflammation and fibrosis, including lymphocyte antigen 6 family member D (*Ly6d*), interleukin 6 (*Il6*), interleukin 1 (*Il1*), tumor necrosis factor α (*Tnfα*), C-C motif chemokine ligand 2 (*Ccl2*), interferon γ (*Ifng*), nitric-oxide synthase 2 (*Nos2*), collagen type I α1 chain (*Col1a1*), and collagen type I α2 chain (*Col1a2*) (Fig. 2*C*). NF-κB signaling is a key regulator that controls inflammation (25). An increase in nuclear translocation of p65 was observed in the livers of $Shp^{Hep-/-}$ mice (Fig. 2*D*), supporting the overall increase of liver inflammation in $Shp^{Hep-/-}$ mice.

Hepatic Shp deletion reduces diet-induced liver steatosis but exacerbates liver inflammation and fibrosis

Our previous study has described a mouse NASH model induced by HFCF diet (17). As shown in Fig. 3*A*, the HFCF diet feeding for 12 weeks did not alter the expression of hepatic *Shp* and its target gene cytochrome P450 family 7 subfamily A member 1 (*Cyp7a1*). We then superimposed hepatic *Shp* deletion by AAV8-Tbg-Cre on an HFCF feeding regimen (Fig. 3*B*). Both $Shp^{Hep-/-}$ mice and WT mice developed glucose intolerance after HFCF diet for 12 weeks (Fig. 3*C*). Meanwhile, body weight gain and fasting serum triglycerides were similar in $Shp^{Hep-/-}$ and WT mice after 12 weeks on the HFCF diet (Fig. 3, *D* and *E*). However, a decrease in fasting serum cholesterol level was observed in HFCF-fed $Shp^{Hep-/-}$ (Fig. 3*E*). In contrast, serum

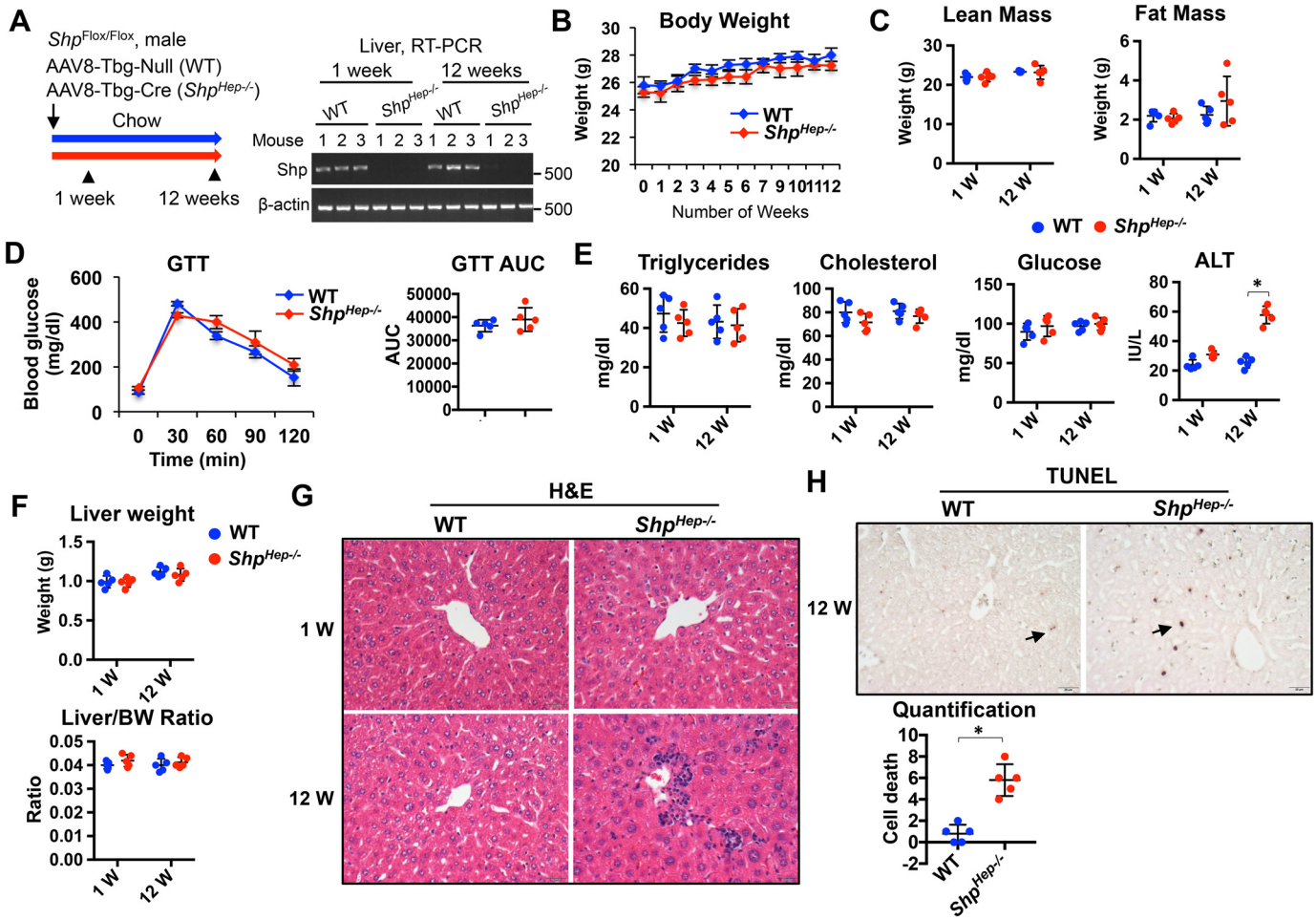

Figure 1. Hepatocyte-specific *Shp* deletion in adult mice induces liver injury. Two-month-old male $Shp^{flox/flox}$ mice were injected with either AAV8-Tbg-Cre or control AAV8-Tbg-null to generate hepatocyte-specific *Shp* knockout ($Shp^{Hep-/-}$) and WT controls, respectively. Samples were collected at 1 week or 12 weeks after AAV8 injection. *A*, *left*, *schematic diagram* showing experimental design. *Right*, RT-PCR analysis of *Shp* mRNA levels in the liver. *B*, mouse body weight change over time. *C*, lean mass and fat mass were determined by the EchoMRI™ system. *D*, *left*, GTTs. *Right*, calculation of area under the curve (*AUC*) of GTT. *E*, fasting serum triglycerides, cholesterol, glucose, and ALT. *F*, liver weight and liver/body weight ratios. *G*, liver H&E stain. *H*, *top*, cell death was detected by TUNEL staining. *Bottom*, quantification of cell death. Data are represented as mean ± S.E. (*error bars*) in *B–F* and *H*. $n = 3–5$ mice/group. *, $p < 0.05$ $Shp^{Hep-/-}$ *versus* WT.

ALT was significantly increased in HFCF-fed $Shp^{Hep-/-}$ mice compared with HFCF-fed WT mice (Fig. 3*E*).

Whole-body $Shp^{-/-}$ mice and hepatocyte-specific $Shp^{-/-}$ mice are resistant to high-fat diet–induced liver steatosis (14, 15). Consistently, a decrease in liver weight and liver/body weight ratio was observed in HFCF-fed $Shp^{Hep-/-}$ mice compared with HFCF-fed WT controls (Fig. 3*F*). Additionally, both Oil Red O staining and liver lipid extraction quantification revealed reduced liver steatosis, triglycerides, and cholesterols in HFCF-fed $Shp^{Hep-/-}$ mice (Fig. 3, *G* and *H*), supporting the overall resistance to diet-induced liver steatosis triggered by hepatic *Shp* deletion.

Shp is a critical suppressor for bile acid synthesis through the direct inhibition of *Cyp7a1* (6, 7), a critical rate-limiting enzyme that converts cholesterol to 7α-hydroxycholesterol for bile acid synthesis (26). Knockout of *Shp* increases bile acid synthesis and decreases hepatic accumulation of cholesterol (27). Consistently, HFCF-fed $Shp^{Hep-/-}$ mice displayed increased bile acid pool size and fecal bile acid excretion rate (Fig. 3*I*) in parallel with the reduction of hepatic and serum cholesterol levels compared with HFCF-fed WT controls (Fig. 3, *E* and *H*). The data indicate that hepatic *Shp* deficiency increases cholesterol conversion for bile acid synthesis and decreases hepatic and serum cholesterol levels subsequently.

In contrast to the attenuation of liver steatosis, *Shp* deletion surprisingly exacerbated liver inflammation and fibrosis during NASH development, evidenced by an increase in macrophage infiltration as well as collagen formation in HFCF-fed $Shp^{Hep-/-}$ liver compared with HFCF-fed WT controls (Fig. 4, *A* and *B*). At mRNA levels, an increase in expression of genes involved in inflammation (*Il6*, *Tnfα*, *Ccl2*, *Il1*, *Ifng*, and *Nos2*) and fibrosis (*Col1a1*, *Col1a2*, *Col5a1*, *Mmp12*, and *Mmp13*) was observed in HFCF-fed $Shp^{Hep-/-}$ liver (Fig. 4*C*). Taken together, these data indicate that hepatocyte-specific *Shp* depletion in adult mice attenuates HFCF diet-induced steatosis but exacerbates liver inflammation and fibrosis.

RNA-Seq reveals activation of inflammatory processes and pathways by hepatic Shp deletion

To pursue an unbiased investigation of mechanisms by which hepatocyte-specific *Shp* deletion induces the disconnec-

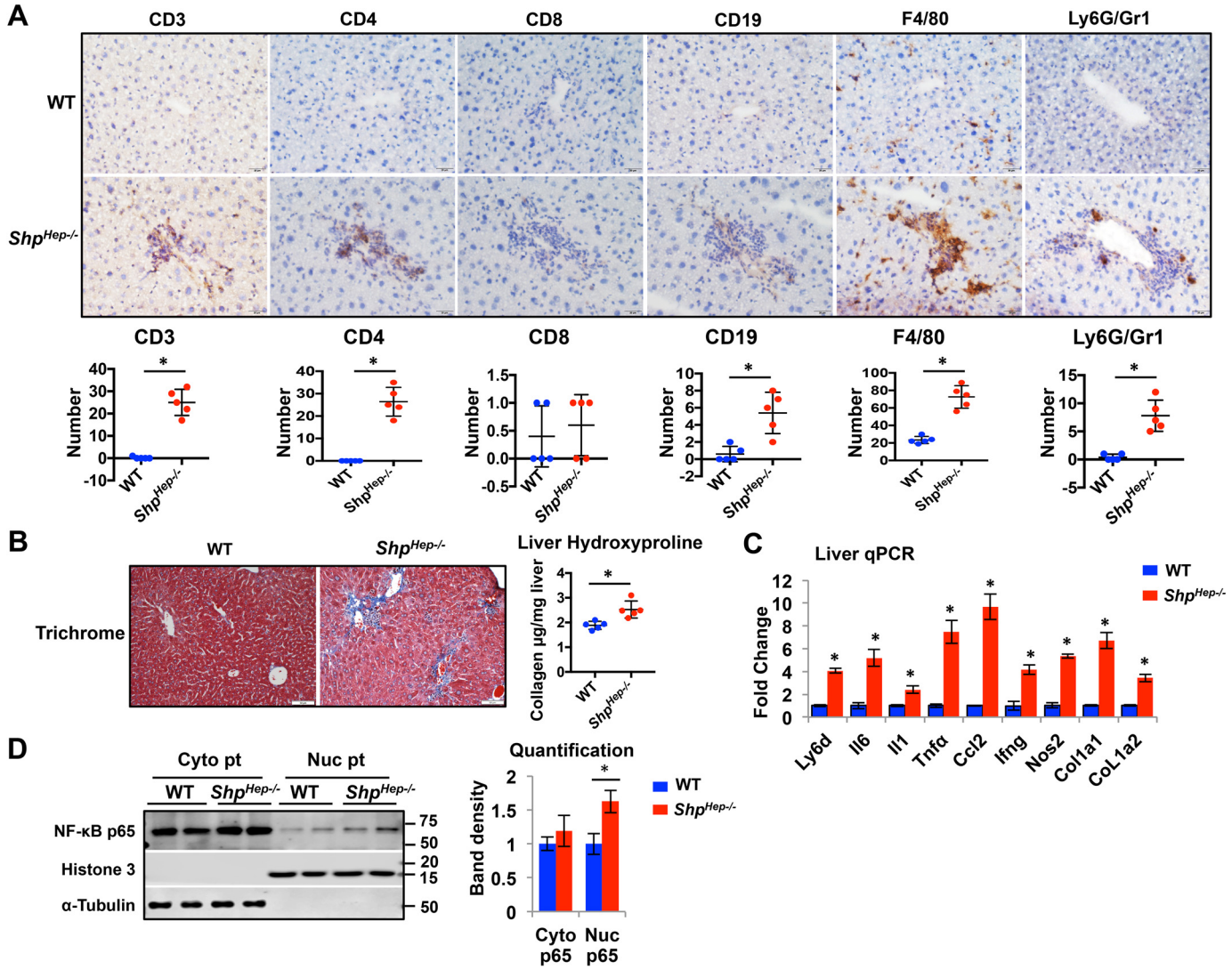

Figure 2. Hepatic Shp disruption induces liver inflammation and fibrosis. Liver samples were collected at 12 weeks after injection of AAV8-Tbg-Cre or control AAV8-Tbg-null. *A*, *top*, representative images of liver sections stained with inflammatory cell markers CD3, CD4, CD8, CD19, F4/80, and Ly6G/Gr1. Original magnification, ×40. *Bottom*, quantification of positive stained cells. *B*, *left*, representative images of liver sections stained with Masson's trichrome. Original magnification, ×40. *Right*, liver collagen content was determined by a hydroxyproline assay. *C*, the relative mRNA levels of genes related to inflammation and fibrosis in liver tissues were determined by qPCR. *D*, *left*, Western blot analysis of cytosolic (*Cyto*) and nuclear (*Nuc*) proteins (*Pt*) in the liver. *Right*, the band intensities of p65 were normalized by loading controls. The expression of p65 in $Shp^{Hep-/-}$ mice relative to that in WT controls is plotted. Data are represented as mean ± S.E. (*error bars*); $n = 5$ mice/group. *, $p < 0.05$ $Shp^{Hep-/-}$ *versus* WT.

tion between steatosis and inflammation in NASH, we conducted RNA-Seq analysis of liver obtained from WT and $Shp^{Hep-/-}$ mice after 12 weeks on the chow and HFCF diet (GEO number: GSE133566). The FPKM was calculated to quantify the expression of genes in four groups, including WT chow, $Shp^{Hep-/-}$ chow, WT HFCF, and $Shp^{Hep-/-}$ HFCF. The differentially expressed genes (DEGs) were determined using a -fold change cutoff of 1.50 and false discovery rate of <0.05.

Under the chow diet, 1,106 genes were significantly differentially expressed between WT and $Shp^{Hep-/-}$ mice ($Shp^{Hep-/-}$ chow *versus* WT chow). After HFCF treatment, a total of 1,352 DEGs were identified in the comparison of $Shp^{Hep-/-}$ HFCF *versus* WT HFCF. Meanwhile, HFCF feeding resulted in 794 DEGs in the comparison of WT HFCF *versus* WT chow and 324 DEGs in the comparison of $Shp^{Hep-/-}$ HFCF *versus* $Shp^{Hep-/-}$ chow, respectively. The volcano plot analysis of gene expression revealed that *Shp* deletion induced major changes in DEGs compared with WT groups, with the greatest effect being that of HFCF diet (Fig. 5*A*).

A heat map with hierarchical clustering was used to determine the expression patterns of DEGs in WT and $Shp^{Hep-/-}$ mice fed a chow or HFCF diet. The idea is that genes with similar expression patterns may have similar functions or may be involved in the same biological process or cellular pathway; therefore, they are clustered into classes. In this study, we found that $Shp^{Hep-/-}$ mice were distinctly separated from WT on both chow and HFCF conditions (Fig. 5*B*). The DEGs in four groups were clustered into two major types, one with higher expression in the WT groups but lower expression in the $Shp^{Hep-/-}$ groups and the other with lower expression in the WT groups but higher expression in the $Shp^{Hep-/-}$ groups.

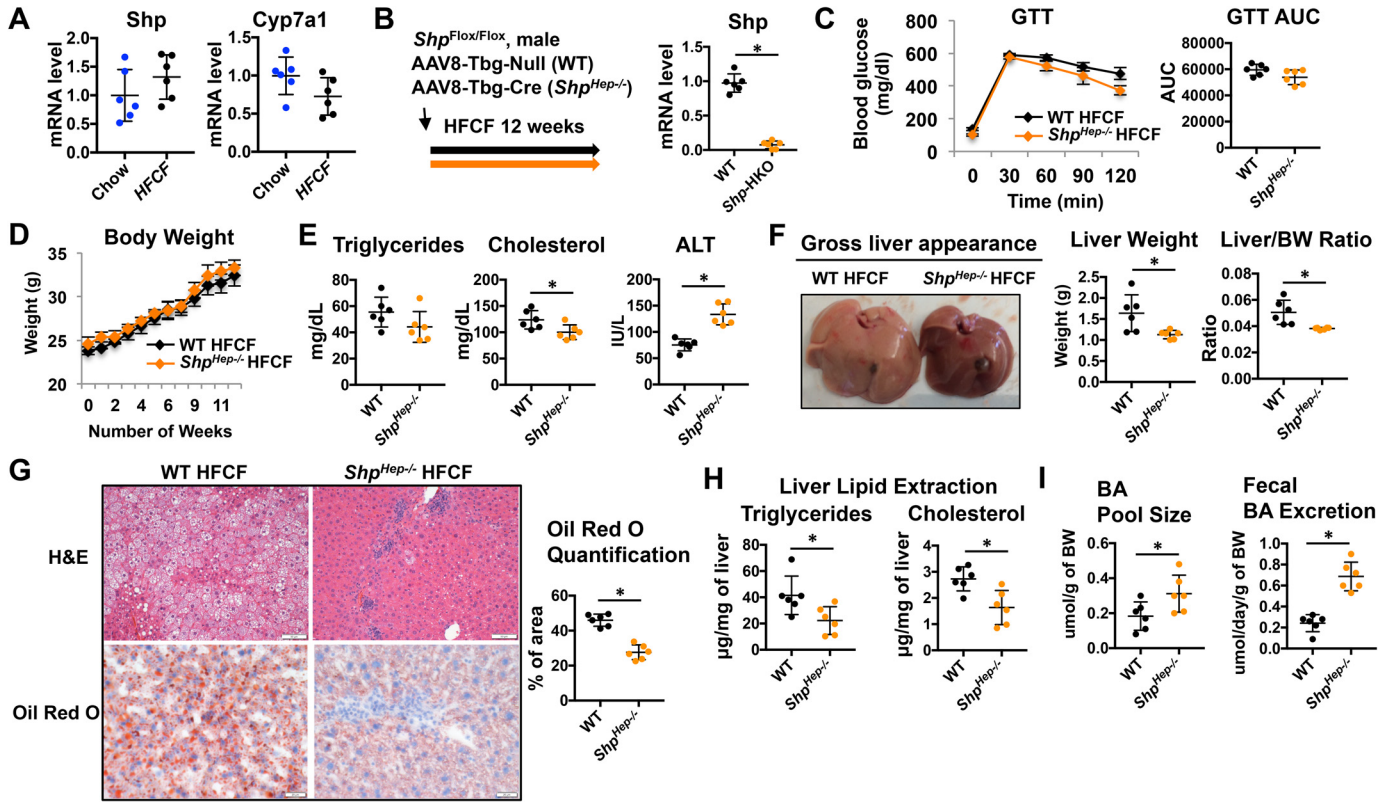

Figure 3. Hepatic *Shp* deficiency attenuates diet-induced liver steatosis. *A*, qPCR analysis of hepatic *Shp* and *Cyp7a1* in mice fed either a chow or HFCF diet for 12 weeks. *B–I*, 2-month-old male $Shp^{flox/flox}$ mice were injected with either AAV8-Tbg-Cre or control AAV8-Tbg-null to generate hepatocyte-specific *Shp* knockout ($Shp^{Hep-/-}$) or WT controls, respectively. Mice were then fed HFCF diet for 12 weeks. *B*, *left*, *schematic diagram* showing experimental design. *Right*, qPCR analysis of *Shp* mRNA levels in the liver. *C*, *left*, GTTs. *Right*, calculation of area under the curve (*AUC*) of GTT. *D*, mouse body weight change over time. *E*, fasting serum triglycerides, cholesterol, and ALT. *F*, *left*, gross liver appearance. *Right*, liver weight and liver/body weight ratio. *G*, *left*, representative images of liver sections stained with H&E and Oil Red O. Original magnification, ×40. *Right*, quantification of Oil Red O staining. *H*, quantification of liver triglycerides and cholesterols from lipid extracts. *I*, bile acid pool size and fecal bile acid excretion rate. Data are represented as mean ± S.E. (*error bars*); $n = 6$ mice/group. *, $p <$ 0.05 $Shp^{Hep-/-}$ HFCF *versus* WT HFCF.

We next conducted gene ontology (GO) enrichment and KEGG (Kyoto Encyclopedia of Genes and Genomes) pathway analysis of DEGs using Enrichr Tools. The DEGs in each group were assigned to GO terms describing biological processes, cellular components, and molecular functions. The enriched GO terms and KEGG pathways with adjusted p values < 0.05 were selected and summarized in the supporting information. As shown in Fig. 6*A*, the GO enrichment analysis indicated that a major effect of genes involved in proinflammatory and fibrogenic processes, such as extracellular matrix organization, cytokine, type I interferon, neutrophil degranulation, and cellular response to interferon γ, were induced by *Shp* deletion under a chow diet. Furthermore, KEGG pathway analysis of DEGs demonstrated that multiple pathways were differentially altered in $Shp^{Hep-/-}$ chow compared with WT chow, with the cytokine-cytokine receptor interaction, hematopoietic cell lineage, chemokine signaling, T cell receptor signaling, and NF-κB signaling as the top five enriched KEGG pathways based on statistical significance (Fig. 6*A*).

The top five biological processes and pathways altered by HFCF diet in WT or $Shp^{Hep-/-}$ mice are displayed in Fig. 6 (*B* and *C*, respectively). Among them are some common metabolic processes and pathways, such as steroid and cholesterol biosynthesis, regulation of triglyceride, and PPAR signaling.

Activation of NF-κB and suppression of Pparg signaling in HFCF-fed $Shp^{Hep-/-}$ mice

To further characterize HFCF diet–induced biological pathways and disease processes that are directly influenced by *Shp* deletion, we compared gene expression between WT HFCF and $Shp^{Hep-/-}$ HFCF (Fig. 6*D*). As expected, biological processes and pathways involved in inflammation (type I interferon, cytokine, exocytosis, chemokine, T cell receptor, NF-κB signaling) were distinctly affected by hepatic disruption of *Shp*. In addition, HFCF-induced PPAR signaling, the key pathway involved in lipid metabolism, was largely impacted by the absence of *Shp* (Fig. 6*D*).

Among genes involved in NF-κB signaling most significantly induced by loss of *Shp* were phosphatidylinositol-4-phosphate 3-kinase catalytic subunit type 2γ (*Pik3c2g*), fibroblast growth factor receptor 1 (*Fgfr1*), NF-κB inhibitor δ (*Nfkbid*), lymphocyte protein-tyrosine kinase (*Lck*), TNFα-induced protein 3 (*Tnfaip3*), interleukin 33 (*Il33*), Toll-like receptor 8 (*Tlr8*), TNF receptor superfamily member 11a (*Tnfrsf11a*), interleukin 1β (*Il1b*), phosphoinositide-3-kinase regulatory subunit 5 (*Pik3r5*), phosphatidylinositol-4,5-bisphosphate 3-kinase catalytic subunit γ (*Pik3cg*), Toll-like receptor 8 (*Tlr2*), phospholipase C γ2 (*Plcg2*), interleukin 1 receptor antagonist (*Il1rn*), caspase recruitment domain family member 11 (*Card11*),

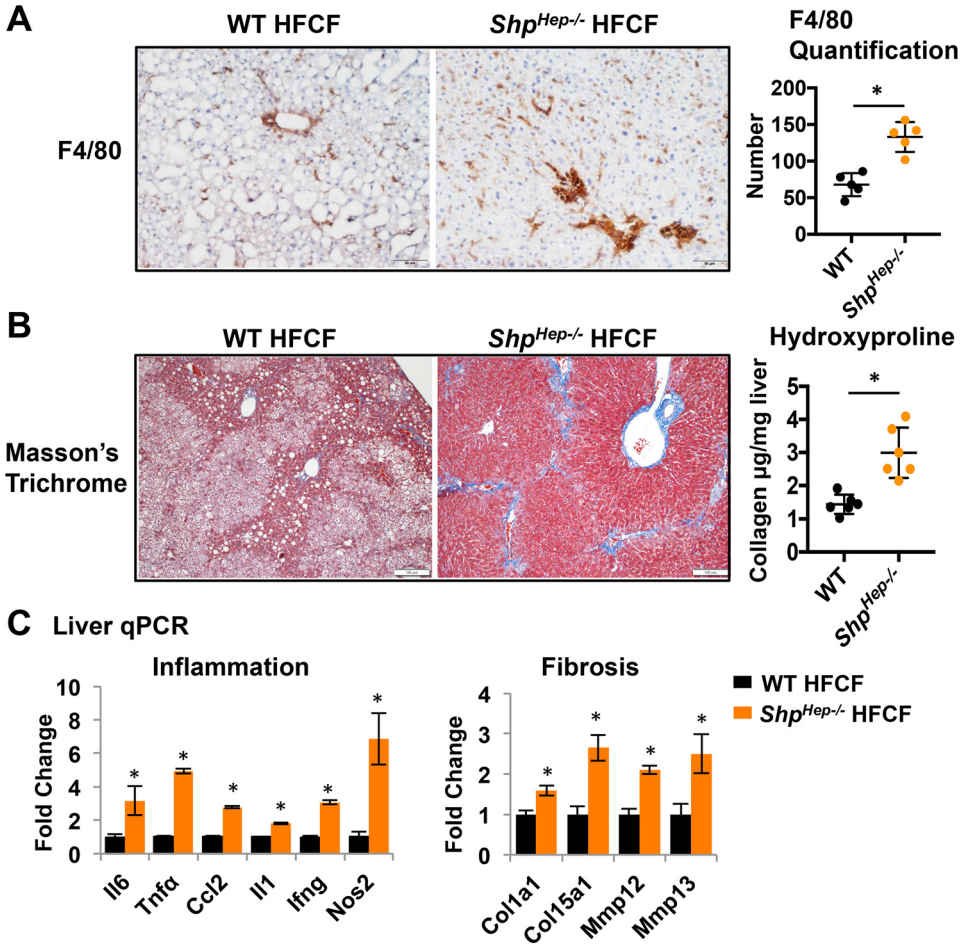

Figure 4. Disruption of *Shp* in hepatocytes exacerbates liver inflammation and fibrosis in HFCF-fed mice. Liver samples were collected from 12-week HFCF-fed $Shp^{Hep-/-}$ and HFCF-fed WT mice. *A*, *left*, representative images of liver sections stained with F4/80. Original magnification, ×40. *Right*, quantification of F4/80-positive cells. *B*, *left*, liver sections stained with Masson's trichrome. *Right*, liver collagen content was determined by a hydroxyproline assay. *C*, relative mRNA levels of genes related to inflammation and fibrosis in liver tissues were determined by qPCR. Data are represented as mean ± S.E. (*error bars*); $n = 6$ mice/group. *, $p < 0.05$ HFCF-fed WT *versus* HFCF-fed $Shp^{Hep-/-}$.

phosphatidylinositol-4,5-bisphosphate 3-kinase catalytic subunit δ (*Pik3cd*), *Cd40*, *Tnfα*, Toll-like receptor 3 (*Tlr3*), mitogen-activated protein kinase kinase kinase 8 (*Map3k8*), and epidermal growth factor receptor (*Egfr*) (Fig. 7*A*). In contrast, neurotrophic receptor tyrosine kinase 1 (*Ntrk1*) was dramatically down-regulated by the hepatic disruption of *Shp* (Fig. 7*A*).

To clarify the causative role of NF-κB signaling in *Shp* deletion-induced inflammation, we isolated hepatocytes from $Shp^{flox/flox}$ mice and deleted *Shp* ($Shp^{-/-}$) using adenovirus expression Cre recombinase. The infection of adenovirus vector control was used to generate WT hepatocytes. The real-time PCR confirmed the successful knockdown of *Shp* in hepatocytes (Fig. 7*B*, *left*). As expected, loss of *Shp* in hepatocytes significantly increased the expression of *Tnfα*, an established NF-κB target (Fig. 7*B*, *right*). Most importantly, the induction of *Tnfα* was markedly inhibited by the treatment of a specific NF-κB inhibitor, BAY 11-7082 (Fig. 7*B*, *right*). The above data indicate that NF-κB activation plays a critical role in *Shp* deletion–induced initiation of inflammation.

Ppar family members (Pparα, Pparβ/δ, and Pparg) control the transcription of genes in lipid and carbohydrate metabolism. As shown in Fig. 8 (*A* and *B*), major genes involved in lipid metabolism, including sterol regulatory element– binding transcription factor 1 (*Srebp1c*), stearoyl-CoA desaturase 1 (*Scd1*), *Pparα*, *Pparg*, and some *Pparg* targets, such as fatty acid–binding protein 1 (*Fabp1*), cell death–inducing DFFA-like effector c (*Cidec*), and *CD36*, were significantly induced in HFCF-fed WT liver but decreased in the absence of hepatic *Shp*. The above data support the overall resistance of $Shp^{Hep-/-}$ mice to HFCF-induced liver steatosis.

SHP has been shown to interact and alter the function of many nuclear receptors in lipid metabolism, including *Pparg*, *Pparα*, *Lrh1*, *Hnf4α*, *Fxr*, *Lxrα*, and *Lxrβ* (11). Strikingly, hepatic *Shp* disruption specifically decreased *Pparg* expression in both chow and HFCF conditions (Fig. 8*C*). In contrast, hepatic *Shp* deletion abolished HFCF-induced up-regulation of *Pparα*, but did not impact *Pparα* expression in the chow-fed mice. Moreover, neither HFCF diet nor *Shp* deletion altered hepatic expression of *Lrh1*, *Hnf4α*, *Fxr*, *Lxrα*, and *Lxrβ* (Fig. 8*C*). PPARg is expressed at a low level in normal liver but markedly increased in fatty liver (28). PPARg overexpression up-regulates various lipogenic genes and promotes liver steatosis, whereas hepatocyte *Pparg* deletion ameliorates liver steatosis (29, 30). Consistently, here we show that hepatic *Shp* deletion results in *Pparg* down-regulation that is correlated with the decrease of liver steatosis.

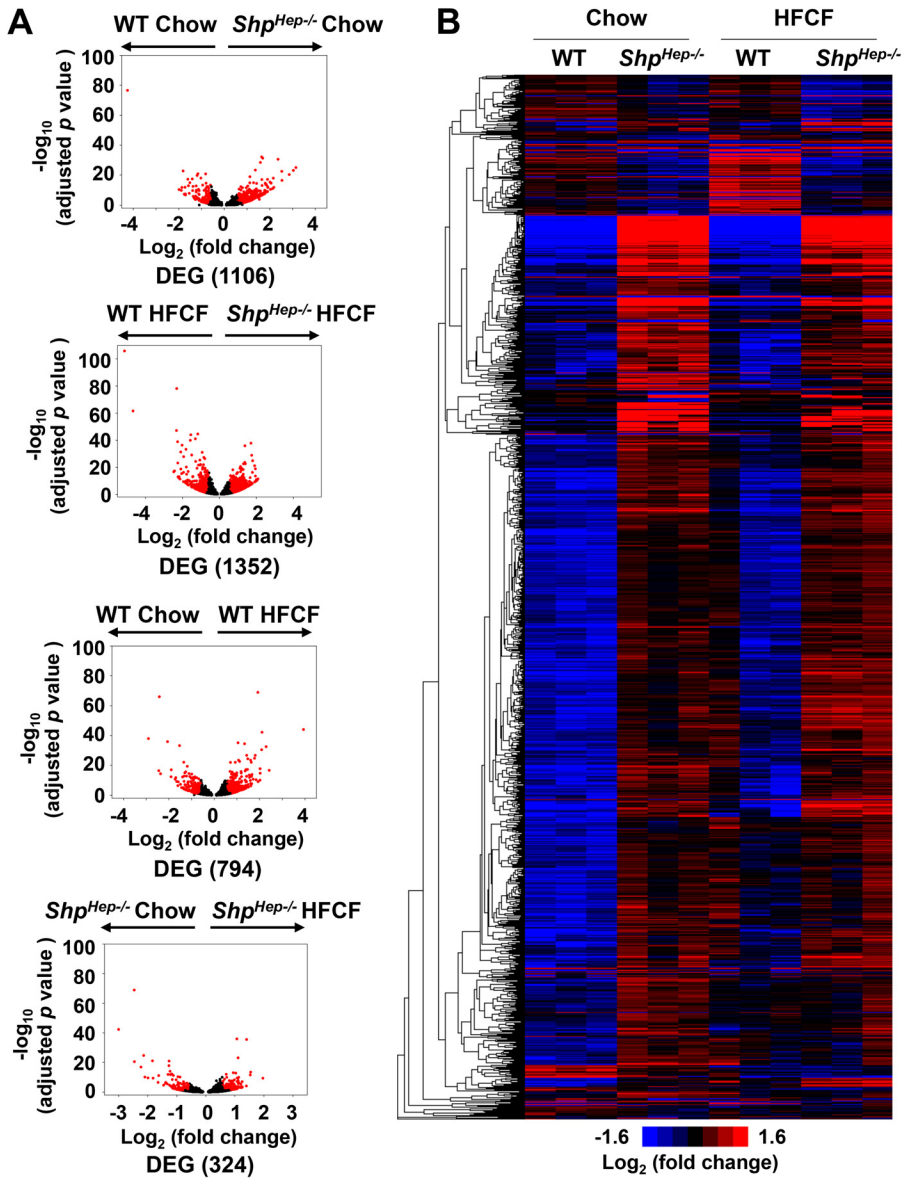

Figure 5. RNA-Seq analysis of liver transcriptome of WT and *Shp*$^{Hep-/-}$ mice after chow or HFCF diet. WT and *Shp*$^{Hep-/-}$ mice were generated by injection of AAV8-Tbg-null or AAV8-Tbg-Cre into 2-month-old *Shp*$^{flox/flox}$ male mice, respectively. Liver samples were collected at 12 weeks after chow or HFCF diet. *A*, volcano plot shows DEGs in the comparison of different groups. *B*, hierarchical clustering of DEGs in WT and *Shp*$^{Hep-/-}$ mice fed chow or HFCF diet.

We next examined *Pparg* and its target gene *Cd36* in WT and *Shp*$^{-/-}$ hepatocytes. As shown in Fig. 8*D*, the mRNA levels of *Pparg* and *Cd36* were significantly decreased in *Shp*$^{-/-}$ hepatocytes compared with WT hepatocytes. We then treated WT and *Shp*$^{-/-}$ hepatocytes with oleic acid (0.5 mM) for 24 h to assess steatosis. Oleic acid dramatically increased steatosis in WT hepatocytes. Strikingly, the lipid accumulation was largely inhibited in *Shp*$^{-/-}$ hepatocytes (Fig. 8*E*). Interestingly, overexpressing *Pparg* by adenovirus greatly increased lipid contents in oleic acid–treated WT hepatocytes, and this response was maintained in *Shp*$^{-/-}$ hepatocytes overexpressed with *Pparg* (Fig. 8*E*). Taken together, the above data clearly indicate that *Pparg* plays a critical role in *Shp* deficiency–induced resistance to steatosis. The overexpression of *Pparg* in WT and *Shp*$^{-/-}$ hepatocytes was confirmed by real-time PCR shown in Fig. 8*F*. Collectively, the above data suggest that *Shp* disruption in hepatocytes activated NF-κB signaling and impaired *Pparg* activation, leading to the progression of liver inflammation and fibrosis with an attenuation of steatosis.

Ablation of hepatic Shp after the development of steatosis enhances liver inflammation and fibrosis in HFCF-fed mice without affecting liver steatosis

In our previous study, we have described that mice fed an HFCF diet for 4 weeks develop liver steatosis without appreciable inflammation or fibrosis (17). We also noticed that 4 weeks of HFCF feeding does not alter hepatic *Shp* expression (17). To investigate the role of *Shp* specifically in the transition of steatosis to NASH, *Shp*$^{flox/flox}$ mice were fed an HFCF diet for 4 weeks followed by *Shp* deletion in hepatocytes by injection of AAV8-Tbg-Cre and remained on the HFCF diet for an additional 8 weeks (Fig. 9*A*). The knockdown of hepatic *Shp* was confirmed by real-time PCR (Fig. 9*A*). No differences in body weight, serum fasting triglycerides, cholesterol, and glucose

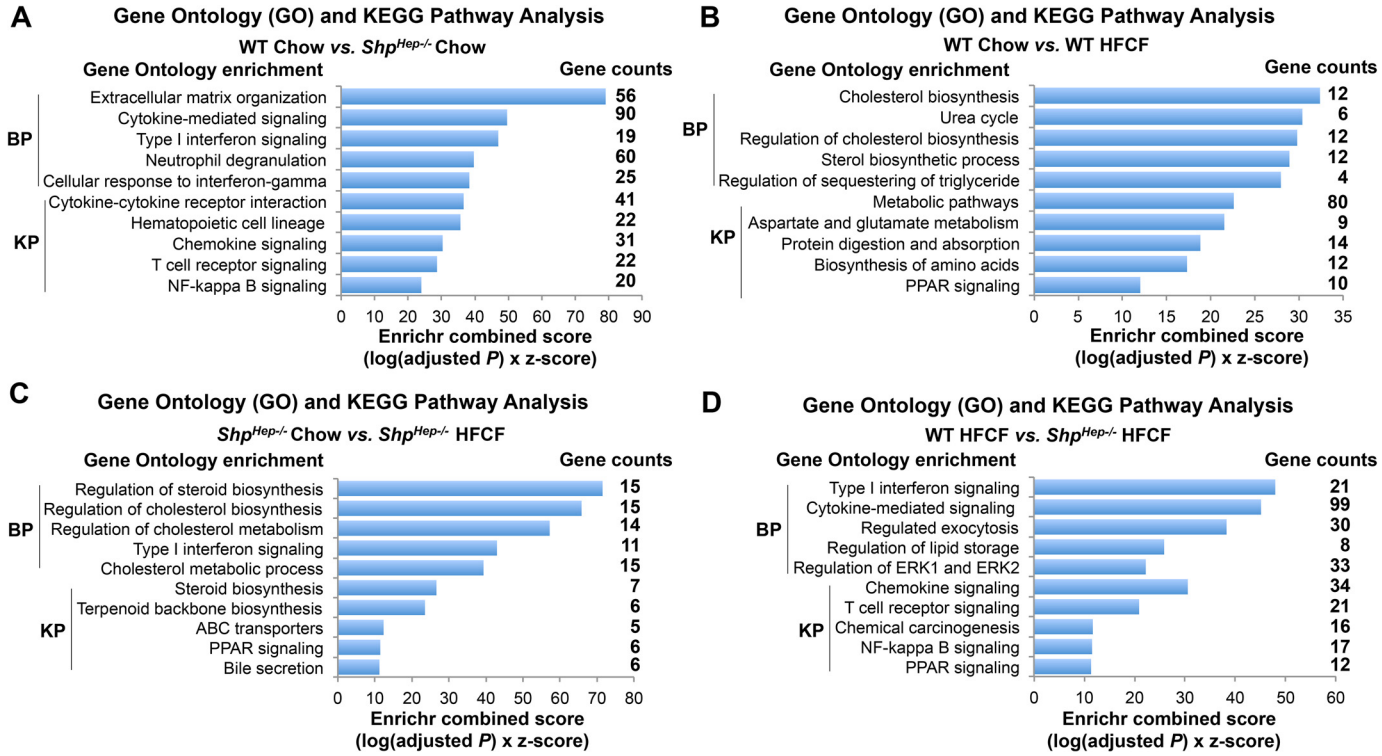

Figure 6. Gene ontology and pathway analysis of DEGs from WT and *Shp*$^{Hep-/-}$ mice after chow or HFCF diet. WT and *Shp*$^{Hep-/-}$ mice were generated by injection of AAV8-Tbg-null or AAV8-Tbg-Cre into 2-month-old *Shp*$^{flox/flox}$ male mice, respectively. RNA-Seq was conducted in liver samples from chow-fed or HFCF-fed mice. The top five enriched biological process (*BP*) terms in gene ontology and top five enriched KEGG pathways (*KP*) in the comparisons of WT chow *versus* *Shp*$^{Hep-/-}$ Chow (*A*), WT chow *versus* WT HFCF (*B*), *Shp*$^{Hep-/-}$ chow *versus* *Shp*$^{Hep-/-}$ HFCF (*C*), or WT HFCF *versus* *Shp*$^{Hep-/-}$ HFCF (*D*) were selected by Enrichr Tools based on Enrichr combined scores.

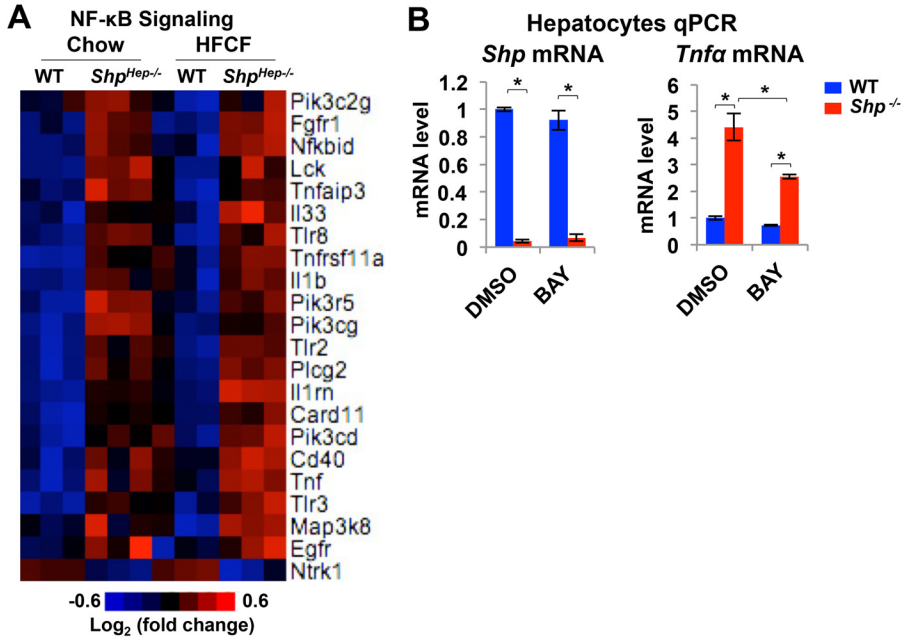

Figure 7. Hepatocyte-specific *Shp* deletion induces NF-κB activation. *A*, heat map depicting DEGs involved in NF-κB signaling by gene ontology enrichment analysis. *B*, the expression of *Shp* and *Tnfα* in mouse hepatocytes was determined by qPCR. Primary hepatocytes from *Shp*$^{flox/flox}$ mice were infected with adenovirus expressing Cre recombinase or vector control to generate *Shp*$^{-/-}$ or WT hepatocytes, respectively. Hepatocytes were then treated with 5 μM NF-κB inhibitor BAY 11-7082 for 6 h. The relative expression of *Shp* or *Tnfα* is normalized to the expression of internal control *Hprt1*. The -fold changes relative to controls are plotted and represented as mean ± S.E. (*error bars*); *, $p < 0.05$. *Shp*$^{-/-}$ *versus* WT.

were noticed between *Shp*$^{Hep-/-}$ and WT controls (Fig. 9, *B* and *C*). However, serum ALT was consistently increased in *Shp*$^{Hep-/-}$ mice (Fig. 9*C*). Interestingly, hepatic *Shp* disruption after steatosis development did not alter liver weight and liver/body weight ratio compared with WT controls (Fig. 9*D*).

Both hematoxylin and eosin (H&E) staining and lipid extraction revealed the similar extent of liver steatosis developed in

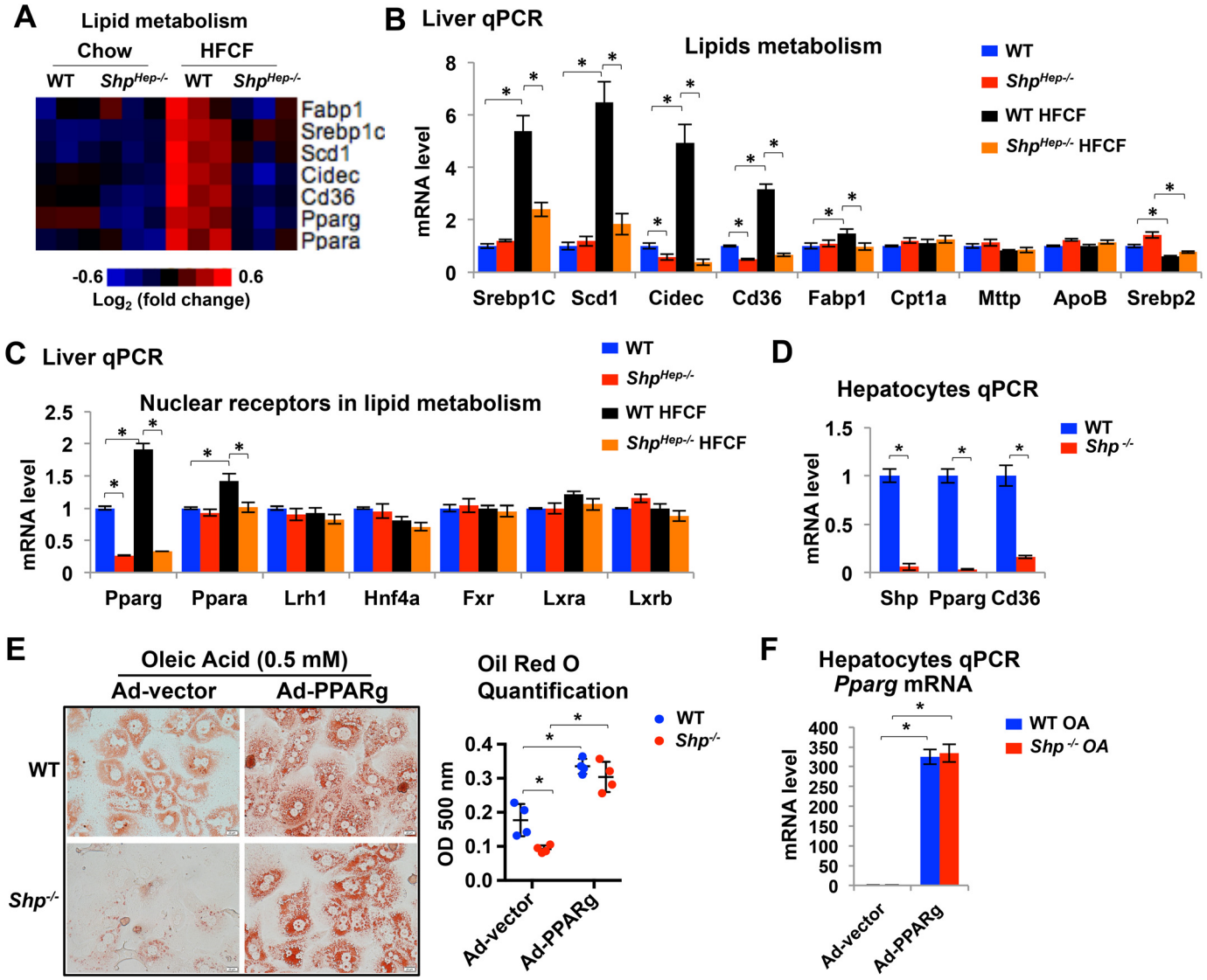

Figure 8. Hepatocyte-specific *Shp* deletion results in Pparg signaling inactivation. *A*, heat map depicting DEGs involved in lipid metabolism by gene ontology enrichment analysis. *B* and *C*, the relative expression of nuclear receptors and genes involved in lipid metabolism in the liver was determined by qPCR. Data are represented as mean ± S.E. (*error bars*); $n = 6$ mice/group. *D*, qPCR analysis of gene expression in mouse hepatocytes. Primary hepatocytes from $Shp^{flox/flox}$ mice were infected with adenovirus expressing Cre recombinase or vector control to generate $Shp^{-/-}$ or WT hepatocytes, respectively. *E*, $Shp^{-/-}$ and WT hepatocytes were infected with adenovirus expressing PPARg (*Ad-PPARg*) or vector control (*Ad-vector*). Cells were then incubated with 0.5 mM oleic acid for 24 h. *Left*, Oil Red O staining of hepatocytes. *Right*, Oil Red O was dissolved and quantified by the measurement of absorbance at $OD_{500\ nm}$. *F*, qPCR analysis of *Pparg* in mouse hepatocytes. The relative *Pparg* expression is normalized to internal control *Hprt1*. The -fold changes relative to controls are plotted and represented as mean ± S.E. (*error bars*); *, $p < 0.05$.

$Shp^{Hep-/-}$ mice and WT controls in this steatosis-to-NASH transition model (Fig. 9*E*). However, the livers of $Shp^{Hep-/-}$ mice displayed a marked increase in F4/80^{+} macrophages and collagen formation (Fig. 9, *F* and *G*). Consistently, the expression of genes involved in inflammation (*Ccl2*, *Tnfα*, and *Nos2*) and fibrosis (*Col1a1* and *Col1a2*) were significantly increased in the livers of HFCF-fed $Shp^{Hep-/-}$ mice (Fig. 9*H*). Next, we examined hepatic *Pparg* expression. Surprisingly, although there were similar levels of liver steatosis in HFCF-fed $Shp^{Hep-/-}$ mice and WT controls, the expression of hepatic *Pparg* was consistently lower in $Shp^{Hep-/-}$ mice (Fig. 9*H*), supporting a strong regulation of *Shp* on *Pparg*'s expression that is independent of liver steatosis. Meanwhile, our data also indicate that after steatosis development, disruption of hepatic *Shp* decreases *Pparg* expression but could not alter liver steatosis; instead, other *Pparg*-independent mechanisms may contribute significantly to liver steatosis. Taken together, the above data support *Shp* as a key player that prevents NASH progression by inhibiting both liver inflammation and fibrosis.

Discussion

Steatosis alone is considered to be little to no risk for progressive liver disease, whereas NASH can progress into irreversible cirrhosis and hepatocellular carcinoma without effective treatments. Given the clinical significance of NASH, identifying key factors and pathways that promote the progression of steatosis to NASH is critically important for developing effective prevention and therapeutic strategies. Using a clinically relevant dietary mouse NASH model, we investigated the role of SHP in NASH development. We demonstrate that disruption of

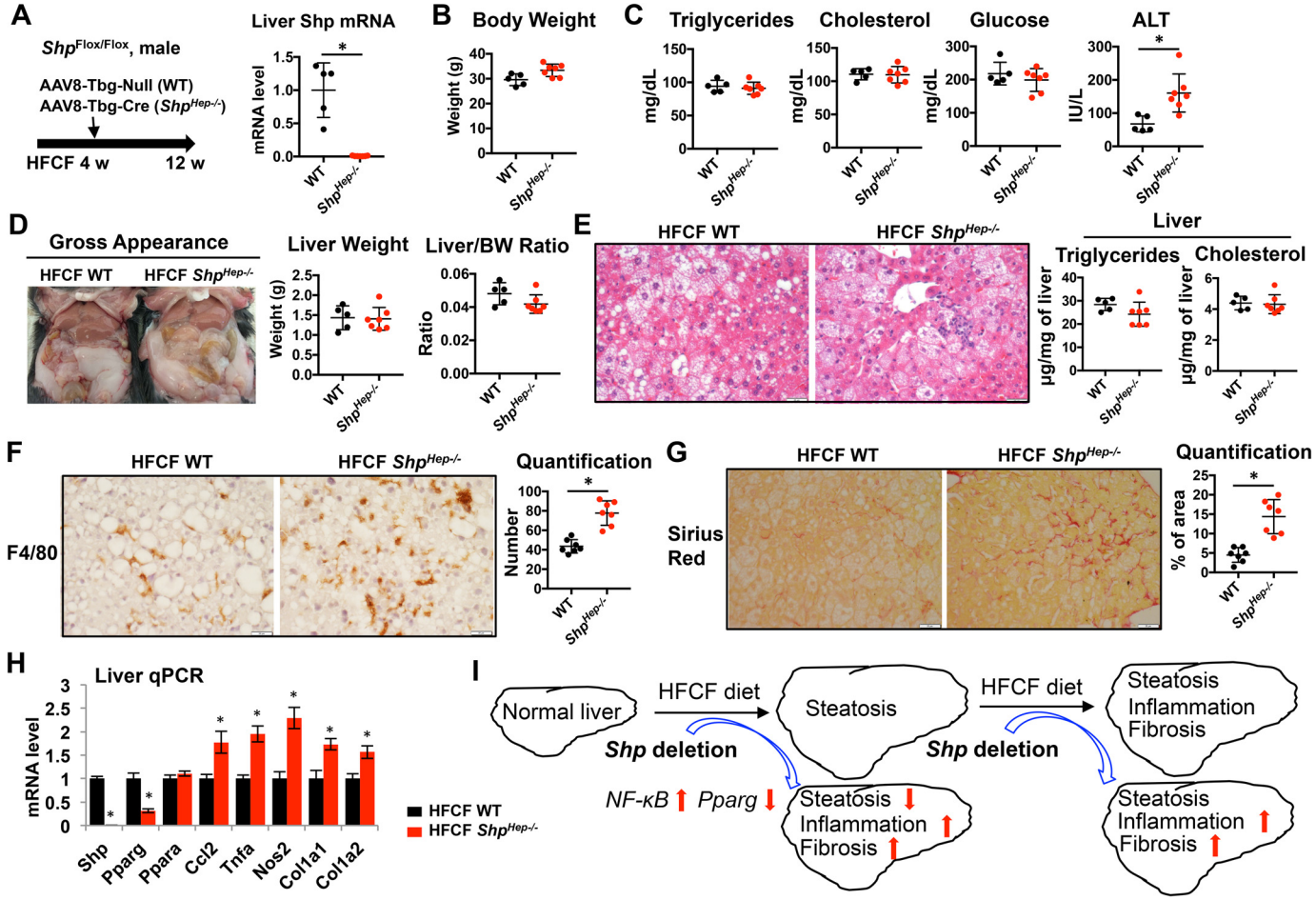

Figure 9. Disruption of hepatic *Shp* after steatosis development exacerbates liver inflammation and fibrosis in HFCF-fed mice. *A–H*, 2-month-old male $Shp^{flox/flox}$ mice were fed an HFCF diet for 4 weeks to develop liver steatosis, followed by tail vein injection of AAV8-Tbg-Cre or AAV8-Tbg-null control. Mice remained on the HFCF diet for an additional 8 weeks. *A*, *left*, *schematic diagram* showing experimental design. *Right*, qPCR analysis of *Shp* mRNA levels in the liver. *B*, body weight. *C*, fasting serum triglycerides, cholesterol, glucose, and ALT. *D*, *left*, gross liver appearance. *Right*, liver weight and liver/body weight ratio. *E*, *left*, representative images of liver sections stained with H&E. Original magnification, ×40. *Right*, quantification of liver triglycerides and cholesterol contents from lipid extracts. *F*, *left*, representative images of liver sections stained with F4/80. Original magnification, ×40. *Right*, quantification of F4/80-positive cells. *G*, representative images of liver sections stained with Picrosirius Red. Original magnification, ×40. *Right*, quantification of Picrosirius Red staining in the liver. *H*, the hepatic expression of genes involved in lipid metabolism, inflammation, and fibrosis was determined by qPCR. Data are represented as mean ± S.E. (*error bars*) in *A–H*. $n = 7$ mice/group. *, $p < 0.05$ HFCF-fed $Shp^{Hep-/-}$ *versus* HFCF-fed WT. *I*, *schematic diagram* illustrates the complex role of Shp in NAFLD. Depending on NAFLD stage, hepatic *Shp* plays an opposing role in regulating steatosis, inflammation, and fibrosis. *Shp* disruption in hepatocytes activates NF-κB signaling and impairs *Pparg* activation, leading to the dissociation of steatosis, inflammation, and fibrosis in NAFLD development. *Shp* deletion after steatosis development exacerbates hepatic inflammation and fibrosis without affecting liver steatosis.

hepatic *Shp* activates NF-κB signaling and impairs *Pparg* activation, leading to the dissociation of steatosis, inflammation, and fibrosis during NAFLD development. Interestingly, ablation of hepatic *Shp* after the development of steatosis exacerbates liver inflammation and fibrosis without affecting steatosis (Fig. 9*I*). Our finding that hepatic *Shp* plays a critical role in the steatosis-to-NASH transition provides some new mechanistic insights into our understanding of NASH pathogenesis and progression and may present a new target for NASH treatment.

An important finding from our current study is that *Shp* disruption in hepatocytes induces liver inflammation, which is supported by several pieces of evidence. First, immunohistochemistry staining confirmed an increase in $CD4^+$ T cells, B cells, macrophages, and neutrophils in the liver after 12 weeks of *Shp* deletion. Second, deletion of *Shp* led to a robust induction of genes involved in liver inflammation, such as *Ly6d*, *Il6*, *Il1*, *Tnfα*, *Ccl2*, *Ifnγ*, and *Nos2*. Most importantly, RNA-Seq revealed that absence of *Shp* significantly altered biological processes and pathways involved in inflammation. Finally, loss of *Shp* induced NF-κB signaling activation in hepatocytes that can be blocked by a specific NF-κB inhibitor.

SHP plays an important anti-inflammatory role in monocytes by negatively regulating inflammation induced by Toll-like receptor 4 (TLR4) or NLRP3 inflammasome (31, 32). Here, we found that in hepatocytes, SHP also plays an anti-inflammatory role. Our finding is important, as the hepatocyte is gradually recognized as a key cell type involved in innate immunity by secreting innate immunity proteins, such as bactericidal proteins, opsonins, iron-sequestering proteins, coagulation factor fibrinogen, and cytokines (33). The dysregulation of these innate immunity proteins contributes significantly to the pathogenesis and progression of chronic liver diseases including NASH. For instance, palmitic acid induces production of proinflammatory cytokine interleukin-8 from hepatocytes, contributing to hepatic inflammation and liver injury subsequently (34). Lipotoxicity induces the release of chemokine

(C*X*C motif) ligand 10 (CXCL10)-bearing vesicles from hepatocytes, resulting in macrophage recruitment into the liver (35). Moreover, in a recent study, hepatocytes were found to secret CXCL1/interleukin-8, which causes neutrophil infiltration and alcoholic liver injury (36).

One well-known powerful pro-inflammatory chemokine is CCL2, or monocyte chemoattractant protein 1 (MCP1), which is responsible for attracting monocytes/macrophages and T cells during liver injury. Increase in CCL2 secretion from hepatocytes has been shown in both alcohol fatty liver disease (37) and obesity-associated NAFLD (38), which exacerbates liver injury and inflammation. Similarly, our recent study demonstrated that disruption of *Shp* in hepatocytes induces NF-κB signaling activation, resulting in CCL2 production and secretion from hepatocytes, leading to macrophage recruitment and pro-inflammatory M1 polarization (17). Consistently, in the current study, *Shp* deletion in hepatocytes also causes liver inflammation *in vivo*. Therefore, we speculate that the increase in CCL2 secretion from *Shp*-deficient hepatocytes may contribute to the liver inflammation developed in $Shp^{Hep-/-}$ mice. Further investigation is warranted to explore whether blocking CCL2 production from hepatocytes or repressing CCL2 function could inhibit or ameliorate liver inflammation developed in $Shp^{Hep-/-}$ mice.

The potential role of SHP in NASH patients has been recognized recently. One study (39) showed that SHP is down-regulated in NASH patients. Similarly, our recent study has determined a decrease of SHP expression during the progression of fatty liver to NASH in patients (17). Additionally, increasing SHP expression by the FXR agonist obeticholic acid has been used in the treatment of NAFLD (40), supporting the notion that approaches inducing SHP would be beneficial for NASH treatment.

However, the role of hepatic *Shp* in the development of mouse NAFLD is somehow controversial. Studies showed that both whole-body *Shp* knockout mice and hepatic *Shp* knockout mice displayed resistance to high-fat diet–induced hepatic steatosis (14, 15, 41). Given that all of these fatty liver models are associated with little or no inflammation and fibrosis, the role of hepatic SHP in mouse NASH still remains obscure. Here, we fed mice a high-fat, -cholesterol, and -fructose diet that induces many biochemical and histopathological hallmarks of NASH, to study the role of SHP in modulating liver steatosis, inflammation, and fibrosis during NASH development. The most striking observation was that hepatic *Shp* disruption induces the dissociation of steatosis, inflammation, and fibrosis during NASH development.

Although the molecular mechanism underlying NASH pathogenesis is incompletely understood, numerous studies have demonstrated that NASH development is attributable to multiple hits, including excessive accumulation of toxic lipids within hepatocytes and other insults, such as macrophage-mediated liver inflammation and hepatic stellate cell (HSC)-mediated liver fibrosis. Because toxic lipid metabolites can promote the overproduction of reactive oxygen species that damage hepatocytes, leading to the release of DAMPs into the microenvironment and resulting in macrophage activation, steatosis is generally believed to be positively associated with liver inflammation and liver injury. However, recent studies indicate that the storage of excessive free fatty acids (FFAs) as triglycerides is unlikely to be the cause of hepatocyte injury in NASH (42). Instead, the triglyceride accumulation within hepatocytes acts as a protective mechanism against fatty acid-induced lipotoxicity, which is in response to lipid overload due to the increases in dietary intake of FFA, *de novo* lipogenesis, adipose lipolysis, and impaired FFA oxidation (43). In support of this notion, inhibiting triglyceride synthesis improves hepatic steatosis but exacerbates liver damage and fibrosis in NASH (44). Genetic or pharmacological inhibition of stearoyl-CoA desaturase-1 (SCD1), the enzyme that converts saturated fatty acids to monounsaturated fatty acids for triglyceride synthesis, sensitizes hepatocytes to saturated fatty acid–induced apoptosis. Consequently, $Scd1^{-/-}$ mice displayed decreased steatosis but markedly increased liver injury and fibrosis during NASH development (42). PPARg, a key modulator of lipid synthesis, is markedly up-regulated in fatty liver (28). Disruption of *Pparg* in hepatocytes reduces liver steatosis but dramatically increases hepatic inflammation after high-fat diet plus binge ethanol (36). Fascinatingly, in the current study, disruption of *Shp* in hepatocytes attenuates steatosis but exacerbates liver inflammation and fibrosis in HFCF-fed mice. Mechanistically, the dissociation between steatosis and inflammation in $Shp^{Hep-/-}$ is accompanied by inactivation of *Pparg* and activation of NF-κB, indicating that hepatic SHP plays an opposing role in liver steatosis and inflammation through modulating both *Pparg* and NF-κB signaling.

To further elucidate the role of SHP specifically in the disease transition from steatosis to NASH, we developed a steatosis-to-NASH transition model where mice were fed an HFCF diet for 4 weeks to induce liver steatosis, followed by disruption of *Shp* in hepatocytes. Interestingly, although *Pparg* expression was consistently decreased in this model, hepatic *Shp* deletion after steatosis development exacerbated liver inflammation and fibrosis without affecting liver steatosis. The above observation is in line with our previous finding that hepatic SHP overexpression in HFCF-fed mice does not affect hepatic lipid contents but greatly attenuates liver inflammation and fibrosis during NASH progression (17). Collectively, our current study reconfirms the critical anti-inflammatory and antifibrotic role of SHP in the progression of fatty liver to NASH.

Shp deletion in hepatocytes causes down-regulation of *Pparg*, suggesting a tight regulatory link between *Shp* and *Pparg* in hepatocytes. The mechanism by which *Shp* regulates the expression of *Pparg* remains incompletely understood. One earlier study demonstrated that SHP increases *Pparg* gene expression through a transcriptional cascade where SHP inhibits hairy and enhancer of split 6 (Hes6), a transcriptional repressor that suppresses *Hnf4α*-induced *Pparg* gene expression (41). Another study showed that in rat immortalized HSC cell line HSC-T6, SHP is recruited to the *Pparg* gene promoter and activates *Pparg* transcription (45). Additionally, increasing SHP expression by 6-ethyl cheno-deoxycholic acid (INT-747) stimulates the expression and activity of *Pparg* in adipocytes (46). These data indicate that SHP is a strong transcriptional regulator of *Pparg*, and multiple mechanisms are implicated in this regulation.

Loss of hepatic *Shp* affects the fibrogenic process in the liver, which is another important observation from our current study. The critical antifibrotic role of *Shp* has been documented in the literature. An earlier study (47) demonstrated that disruption of *Shp* exacerbates bile duct ligation–induced cholestatic liver fibrosis, whereas *Shp* overexpression or increasing *Shp* expression by pharmacological compounds attenuates hepatic fibrosis induced either by hepatitis C virus infection (48) or by carbon tetrachloride and α-naphthyl-isothiocyanate (49). In addition, increasing *Shp* mRNA levels in HSCs by FXR ligands abrogates thrombin– and TGF-β1–induced up-regulation of α1 collagen mRNA (50). Furthermore, *Shp* overexpression in HSCs inhibits the expression of tissue metalloproteinase inhibitor 1 (*Timp1*) and promotes a quiescent phenotype of HSCs (51). All of these findings indicate that SHP acts as a critical antifibrotic factor in various liver diseases. Our results, obtained from hepatic *Shp*–deficient animals, support this notion.

In summary, our study provides compelling evidence that hepatic *Shp* disruption in adult mice induces the dissociation of steatosis, inflammation, and fibrosis during NASH development. The complex effects of SHP on hepatic steatosis, inflammation, and fibrosis compromise the potential use of SHP as a therapeutic target for NAFLD treatment. Approaches targeting SHP should be used cautiously, because inhibition of hepatic SHP, although beneficial for the amelioration of liver steatosis, could exacerbate liver inflammation and fibrosis.

Experimental procedures

Antibodies

The following antibodies were used for Western blotting and immunohistochemistry staining: β-actin (Sigma, A-1978), α-tubulin (Sigma, T6074), histone H3 (Cell Signaling, 14269), NF-κB p65 (Cell Signaling, 8242), CD3 (Bio-Rad, MCA500GT), CD4 (Bio-Rad, MCA2691T), CD8 (Bio-Rad, MCA2694T), CD19 (Bio-Rad, MCA1439T), F4/80 (Bio-Rad, MCA497R), and Ly6G/Gr1 (Bio-Rad, MCA2387T).

Animal studies

$Shp^{flox/flox}$ mice were generously provided by Drs. Johan Auwerx and Kristina Schoonjans at the Ecole Polytechnique de Lausanne and backcrossed into C57BL/6J background for 10 generations (17). Mice were maintained in a 12-h light/dark cycle (light on from 6 a.m. to 6 p.m.), temperature-controlled (23 °C), and virus-free facility with free access to food and water. Experiments on mice were performed on males at the age of 8–10 weeks unless stated otherwise ($n = 5–6$/group). To generate hepatocyte-specific *Shp* knockout ($Shp^{Hep-/-}$) and WT controls, $Shp^{flox/flox}$ mice were administered with either adeno-associated virus serotype 8 (AAV8) expressing Cre recombinase driven by the thyroxine-binding globulin (Tbg) promoter (AAV8-Tbg-Cre) or control AAV8 (AAV8-Tbg-null) at a dose of 2×10^{11} genome copies/mouse through tail vein injection. Both AAV8-Tbg-Cre (AV-8-PV1090) and AAV8-Tbg-null (AV-8-PV0148) were obtained from the University of Pennsylvania Vector Core. In dietary NAFLD models, mice were placed on a diet enriched in high fat, cholesterol, and fructose (HFCF; Research Diet, D09100301, 40 kcal% fat, 2% cholesterol, 20 kcal% fructose) for 12 weeks. In a steatosis-to-NASH transition model, $Shp^{flox/flox}$ mice were fed an HFCF diet for 4 weeks to develop liver steatosis, followed by tail vein injection of AAV8-Tbg-Cre or AAV8-Tbg-null control. Mice remained on the HFCF diet for an additional 8 weeks. Mice fed normal chow served as controls. Blood and liver samples were collected after mice had been fasted for 16 h. All experiments were performed in accordance with relevant guidelines and regulations approved by the Institutional Animal Care and Use Committee at the University of Kansas Medical Center.

Glucose tolerance test

Mice were fasted for 16 h, followed by intraperitoneal injection of glucose (2 g/kg body weight). Blood was collected by tail vein puncture. Glucose levels were determined before and at 0.5, 1, 1.5, and 2 h after glucose administration.

Serum measurements

Animals were fasted for 16 h, and blood was collected via cardiac puncture and deposited into blood collection tubes (Fisher, 22-225516). Serum was isolated, and kits were used to measure triglycerides (Pointe Scientific, T7532), total cholesterol (Pointe Scientific, C7510), ALT (Pointe Scientific, A7526), and glucose (Pointe Scientific, G7521).

Liver histological examinations of steatosis, cell death, inflammation, and fibrosis

Fresh liver tissues were fixed with 10% formalin (Fisher, SF100). Paraffin sections at 4 μm were stained with H&E. TUNEL staining for detection of cell death in the liver was performed using an *in situ* cell death detection kit-alkaline phosphatase (Sigma, 11684809910) according to the manufacturer's suggestions. For Oil Red O staining of liver lipids, fresh liver tissue was immediately embedded in Tissue-Tek O.C.T. compound (VWR, 25608-930), and frozen sections were cut at 8 μm, fixed by 10% formalin, and stained with Oil Red O (Sigma, O0625). Images were acquired with a BX60 microscope (Olympus, Lake Success, NY). For immunohistochemical staining, 6-μm frozen sections were fixed by 10% formalin and treated with 0.3% H_2O_2 in methanol for 15 min to block endogenous peroxidase activity. Slides were then treated with 10% normal serum for 30 min, followed by incubation with primary antibody overnight at 4 °C. The ImmPRESS peroxidase polymer detection kit (Vector Laboratories, MP-7444) and ImmPACT 3,3′-diaminobenzidine peroxidase substrate (Vector Laboratories, SK-4105) were used for the final detection. Sections were then counterstained with hematoxylin, dehydrated, cleared, and mounted. Images were acquired with a BX60 microscope. For Picrosirius Red staining of liver fibrosis, 4-μm paraffin sections were rehydrated and incubated in 0.1% Sirius Red F3B (Sigma, Direct Red 80, 365548) containing saturated picric acid (Sigma, p6744) for 1 h. After washing three times in 0.5% glacial acetic acid, sections were briefly dehydrated, cleared, and mounted. Images were acquired with a BX60 microscope, and collagen density was quantified using ImageJ software.

Hepatic triglycerides and cholesterol measurements

According to our previous publication (17), 100 mg of liver tissues were homogenized in 300 μl of chloroform/methanol

(1:2, v/v) for 2 min, followed by a second homogenization for 30 s with an addition of 300 μl of chloroform. The homogenates were mixed with 100 μl of H_2O and homogenized again for 30 s. The lipid layer (~600 μl) was separated via centrifugation at 800 $\times$ *g* for 10 min at room temperature. The lower phase enriched in lipid was transferred and dried using nitrogen gas. The lipid extract was suspended in 300 μl of 5% Triton X-100 in PBS (pH 7.4). The measurement was performed using respective kits for triglycerides (Pointe Scientific, T7532) and cholesterol (Pointe Scientific, C7510). The hepatic triglycerides or cholesterol content was defined as μg of triglycerides or cholesterol per mg of liver tissue.

Analysis of bile acid (BA) pool size and fecal BA extraction rate

To determine BA pool size, fresh mouse tissues including gallbladder, liver, and entire small intestine were minced and extracted in 75% ethanol at 50 °C for 2 h. The extract was then centrifuged, diluted with 75% ethanol, and further diluted with 25% PBS before the BA measurement using a BA colorimetric assay BQ kit (Thermo Fisher Scientific, BQ092A-EALD). The pool size was expressed as μmol of bile acid/g of body weight. To determine fecal bile acid excretion, the feces from individually housed mouse over a 72-h period were collected, weighed, dried, and extracted in 75% ethanol. The extract was then diluted with 25% PBS and subjected to bile acid measurement. The daily fecal output (g/day/g of body weight) and fecal bile acid content (μmol/g) were used to calculate the rate of bile acid excretion (μmol/day/g of body weight).

Determination of hepatic collagen content by hydroxyproline assay

Liver tissues (10 mg) were homogenized in 100 μl of H_2O. The homogenates were mixed with 100 μl of 12 M HCl and incubated at 120 °C for 3 h for acid hydrolysis. The homogenates were then centrifuged at 10,000 $\times$ *g* for 10 min. Aliquots of the hydrolyzed samples (10 μl) were incubated with 100 μl of chloramine T solution (1.27% chloramine T and 10% isopropyl alcohol in acetate-citrate buffer, pH 6.0) at room temperature for 25 min, followed by a second incubation with 100 μl of Ehrlich's solution (Sigma, 03891) at 60 °C for 35 min. A plate reader measured sample absorbance at 550 nm. The hepatic collagen content was defined as μg of collagen per mg of liver tissue.

Western blotting

Nuclear and cytoplasmic protein extraction was carried out using a commercial kit (Fisher, PI78833). Protein lysates (60 μg) were resolved by SDS-PAGE and transferred to nitrocellulose membranes. Membranes were then blocked and incubated with primary antibodies, followed by horseradish peroxidase–conjugated corresponding secondary antibody incubation. Antibody binding was visualized using either SuperSignal West Pico Plus Chemiluminescent Substrate (Fisher, PI34580) or SuperSignal West Femto Chemiluminescent Substrate (Fisher, PI34094). Images were captured by LI-COR, and equal loading of protein was verified by loading controls such as α-tubulin and histone H3. Quantitative analysis of band intensity was performed by Image Studio Lite software, and relative expression levels were normalized to the loading controls.

RNA isolation and RNA-Seq

Total RNA for Illumina sequencing was extracted from mouse liver tissues using a Direct-zol RNA kit (Zymo Research, R2071) according to the manufacturer's protocol. During RNA isolation, DNA was removed by treating the samples with RNase-free DNase to avoid DNA contamination. The purity, concentration, and integrity of the RNA were examined using a NanoDrop 1000 spectrophotometer (Thermo Fisher) and an Agilent Bioanalyzer 2100 system (Agilent Technologies). Three biological replicates in each group for a total of 12 samples were submitted for RNA-Seq. The RNA integrity number values of all samples used for RNA-Seq were >6.0. The high-throughput genomics core at the Huntsman Cancer Institute, University of Utah, performed library preparation and sequencing. cDNA libraries were prepared using the Illumina TruSeq stranded RNA kit with Ribo-Zero Gold. Fifty-cycle single-read sequencing was performed with an Illumina (San Diego, CA) HiSeq 2500, and reads were aligned to a mouse reference sequence genome mm10 using the Novalign short-read alignment software. Sample reads were visualized, and DEGs were identified based on the log-transformed false discovery rate of >1.3 and $\geq \pm 1.5$-fold change in expression relative to controls using the USeq application as described previously (52).

GO and KEGG enrichment analysis of differentially expressed genes

DEGs were used for GO and KEGG (Kyoto Encyclopedia of Genes and Genomes) enrichment analyses on the Enrichr web server to identify biological functions and significantly enriched pathways (53, 54). Enrichr is freely available at http://amp.pharm.mssm.edu/Enrichr.[3] In this study, both GO terms and KEGG pathways with adjusted *p* value <0.05 were considered significantly enriched. An Enrichr combined score was used to select top altered GO terms and KEGG pathways.

Real-time quantitative PCR

The real-time quantitative PCR (qPCR) was carried out using the SYBR Green PCR master mix (Applied Biosystems) as described previously (55). The specific primers are shown in the supporting information. The amount of PCR products was measured by threshold cycle (*Ct*) values, and the relative ratio of specific genes to the housekeeping gene hypoxanthine guanine phosphoribosyl transferase 1 (*Hprt1*) was calculated and presented as -fold change in the tested group relative to the control group.

Mouse primary hepatocyte culture and adenovirus infection

The University of Kansas Medical Center Cell Isolation Core conducted hepatocyte isolation from $Shp^{flox/flox}$ mice using the method described previously (56) with a slight modification. In brief, mouse liver was perfused with 25 ml of solution I (9.5 g/liter Hanks' balanced salt solution, 0.5 mmol/liter EGTA, pH 7.2), followed by 50 ml of solution II (9.5 g/liter Hanks' balanced salt solution, 0.14 g/liter collagenase IV, and 40 mg/liter trypsin inhibitor, pH 7.5). After digestion, single-cell suspension was filtered through a 100-μm Falcon cell strainer (Fisher, 08-771-

[3] Please note that the JBC is not responsible for the long-term archiving and maintenance of this site or any other third party hosted site.

19), and the cells were centrifuged at 50 × *g* for 5 min at 4 °C to pellet hepatocytes. Hepatocytes were then seeded in collagen type 1–coated dishes. After a 2-h incubation, cell culture medium was replaced by fresh William E medium (Sigma, W4128) with various adenoviruses at a multiplicity of infection of 20. The *Pparg* adenovirus (catalog no. 1354), Cre adenovirus (catalog no. 1045), and vector control adenovirus (catalog no. 1240) were purchased from Vector Biolabs. At the second day, hepatocytes were treated either with 5 μM NF-κB inhibitor BAY 11-7082 (Sigma, B5556) for 6 h or with 0.5 mM oleic acid (Sigma, O1008) conjugated with BSA (Fisher, BP9704-100) for 24 h. Cells were then collected for RNA isolation or Oil Red O staining.

Statistical analysis

Quantitative data are presented as the mean ± S.E. The statistically significant difference in data obtained between two groups was determined by Student's *t* test. Multiple groups were compared by one-way ANOVA, followed by Duncan's test. Statistical significance was accepted within 95% confidence limits.

Author contributions—N. M., A. Z., and D. D. formal analysis; N. M., A. Z., P. G., F. A., and Y. Z. investigation; N. M. and A. Z. methodology; N. M., D. D., and Y. Z. writing-review and editing; D. D. data curation; Y. Z. supervision; Y. Z. funding acquisition; Y. Z. writing-original draft; Y. Z. project administration.

References

1. Younossi, Z. M., Koenig, A. B., Abdelatif, D., Fazel, Y., Henry, L., and Wymer, M. (2016) Global epidemiology of nonalcoholic fatty liver disease—Meta-analytic assessment of prevalence, incidence, and outcomes. *Hepatology* **64,** 73–84 CrossRef Medline
2. Wong, V. W., Wong, G. L., Choi, P. C., Chan, A. W., Li, M. K., Chan, H. Y., Chim, A. M., Yu, J., Sung, J. J., and Chan, H. L. (2010) Disease progression of non-alcoholic fatty liver disease: a prospective study with paired liver biopsies at 3 years. *Gut* **59,** 969–974 CrossRef Medline
3. Pais, R., Charlotte, F., Fedchuk, L., Bedossa, P., Lebray, P., Poynard, T., Ratziu, V., and LIDO Study Group (2013) A systematic review of follow-up biopsies reveals disease progression in patients with non-alcoholic fatty liver. *J. Hepatol.* **59,** 550–556 CrossRef Medline
4. McPherson, S., Hardy, T., Henderson, E., Burt, A. D., Day, C. P., and Anstee, Q. M. (2015) Evidence of NAFLD progression from steatosis to fibrosing-steatohepatitis using paired biopsies: implications for prognosis and clinical management. *J. Hepatol.* **62,** 1148–1155 CrossRef Medline
5. Seol, W., Choi, H. S., and Moore, D. D. (1996) An orphan nuclear hormone receptor that lacks a DNA binding domain and heterodimerizes with other receptors. *Science* **272,** 1336–1339 CrossRef Medline
6. Goodwin, B., Jones, S. A., Price, R. R., Watson, M. A., McKee, D. D., Moore, L. B., Galardi, C., Wilson, J. G., Lewis, M. C., Roth, M. E., Maloney, P. R., Willson, T. M., and Kliewer, S. A. (2000) A regulatory cascade of the nuclear receptors FXR, SHP-1, and LRH-1 represses bile acid biosynthesis. *Mol. Cell* **6,** 517–526 CrossRef Medline
7. Lu, T. T., Makishima, M., Repa, J. J., Schoonjans, K., Kerr, T. A., Auwerx, J., and Mangelsdorf, D. J. (2000) Molecular basis for feedback regulation of bile acid synthesis by nuclear receptors. *Mol. Cell* **6,** 507–515 CrossRef Medline
8. Wang, L., Liu, J., Saha, P., Huang, J., Chan, L., Spiegelman, B., and Moore, D. D. (2005) The orphan nuclear receptor SHP regulates PGC-1α expression and energy production in brown adipocytes. *Cell Metab.* **2,** 227–238 CrossRef Medline
9. Suh, Y. H., Kim, S. Y., Lee, H. Y., Jang, B. C., Bae, J. H., Sohn, J. N., Bae, J. H., Suh, S. I., Park, J. W., Lee, K. U., and Song, D. K. (2004) Overexpression of short heterodimer partner recovers impaired glucose-stimulated insulin secretion of pancreatic β-cells overexpressing UCP2. *J. Endocrinol.* **183,** 133–144 CrossRef Medline
10. Kim, Y. D., Park, K. G., Lee, Y. S., Park, Y. Y., Kim, D. K., Nedumaran, B., Jang, W. G., Cho, W. J., Ha, J., Lee, I. K., Lee, C. H., and Choi, H. S. (2008) Metformin inhibits hepatic gluconeogenesis through AMP-activated protein kinase-dependent regulation of the orphan nuclear receptor SHP. *Diabetes* **57,** 306–314 CrossRef Medline
11. Zhang, Y., Hagedorn, C. H., and Wang, L. (2011) Role of nuclear receptor SHP in metabolism and cancer. *Biochim. Biophys. Acta* **1812,** 893–908 CrossRef Medline
12. Nishigori, H., Tomura, H., Tonooka, N., Kanamori, M., Yamada, S., Sho, K., Inoue, I., Kikuchi, N., Onigata, K., Kojima, I., Kohama, T., Yamagata, K., Yang, Q., Matsuzawa, Y., Miki, T., *et al.* (2001) Mutations in the small heterodimer partner gene are associated with mild obesity in Japanese subjects. *Proc. Natl. Acad. Sci. U.S.A.* **98,** 575–580 CrossRef Medline
13. Boulias, K., Katrakili, N., Bamberg, K., Underhill, P., Greenfield, A., and Talianidis, I. (2005) Regulation of hepatic metabolic pathways by the orphan nuclear receptor SHP. *EMBO J.* **24,** 2624–2633 CrossRef Medline
14. Huang, J., Iqbal, J., Saha, P. K., Liu, J., Chan, L., Hussain, M. M., Moore, D. D., and Wang, L. (2007) Molecular characterization of the role of orphan receptor small heterodimer partner in development of fatty liver. *Hepatology* **46,** 147–157 CrossRef Medline
15. Akinrotimi, O., Riessen, R., VanDuyne, P., Park, J. E., Lee, Y. K., Wong, L. J., Zavacki, A. M., Schoonjans, K., and Anakk, S. (2017) Small heterodimer partner deletion prevents hepatic steatosis and when combined with farnesoid X receptor loss protects against type 2 diabetes in mice. *Hepatology* **66,** 1854–1865 CrossRef Medline
16. Benet, M., Guzmán, C., Pisonero-Vaquero, S., García-Mediavilla, M. V., Sánchez-Campos, S., Martínez-Chantar, M. L., Donato, M. T., Castell, J. V., and Jover, R. (2015) Repression of the nuclear receptor small heterodimer partner by steatotic drugs and in advanced nonalcoholic fatty liver disease. *Mol. Pharmacol.* **87,** 582–594 CrossRef Medline
17. Zou, A., Magee, N., Deng, F., Lehn, S., Zhong, C., and Zhang, Y. (2018) Hepatocyte nuclear receptor SHP suppresses inflammation and fibrosis in a mouse model of nonalcoholic steatohepatitis. *J. Biol. Chem.* **293,** 8656–8671 CrossRef Medline
18. Trevaskis, J. L., Griffin, P. S., Wittmer, C., Neuschwander-Tetri, B. A., Brunt, E. M., Dolman, C. S., Erickson, M. R., Napora, J., Parkes, D. G., and Roth, J. D. (2012) Glucagon-like peptide-1 receptor agonism improves metabolic, biochemical, and histopathological indices of nonalcoholic steatohepatitis in mice. *Am. J. Physiol. Gastrointest. Liver Physiol.* **302,** G762–G772 CrossRef Medline
19. Clapper, J. R., Hendricks, M. D., Gu, G., Wittmer, C., Dolman, C. S., Herich, J., Athanacio, J., Villescaz, C., Ghosh, S. S., Heilig, J. S., Lowe, C., and Roth, J. D. (2013) Diet-induced mouse model of fatty liver disease and nonalcoholic steatohepatitis reflecting clinical disease progression and methods of assessment. *Am. J. Physiol. Gastrointest. Liver Physiol.* **305,** G483–G495 CrossRef Medline
20. Kohli, R., Kirby, M., Xanthakos, S. A., Softic, S., Feldstein, A. E., Saxena, V., Tang, P. H., Miles, L., Miles, M. V., Balistreri, W. F., Woods, S. C., and Seeley, R. J. (2010) High-fructose, medium chain trans fat diet induces liver fibrosis and elevates plasma coenzyme Q9 in a novel murine model of obesity and nonalcoholic steatohepatitis. *Hepatology* **52,** 934–944 CrossRef Medline
21. Magee, N., Zou, A., and Zhang, Y. (2016) Pathogenesis of nonalcoholic steatohepatitis: interactions between liver parenchymal and nonparenchymal cells. *Biomed Res. Int.* **2016,** 5170402 CrossRef Medline
22. Cohen, J. C., Horton, J. D., and Hobbs, H. H. (2011) Human fatty liver disease: old questions and new insights. *Science* **332,** 1519–1523 CrossRef Medline
23. Schuppan, D., and Schattenberg, J. M. (2013) Non-alcoholic steatohepatitis: pathogenesis and novel therapeutic approaches. *J. Gastroenterol. Hepatol.* **28,** Suppl. 1, 68–76 CrossRef Medline
24. Sun, Z., Miller, R. A., Patel, R. T., Chen, J., Dhir, R., Wang, H., Zhang, D., Graham, M. J., Unterman, T. G., Shulman, G. I., Sztalryd, C., Bennett, M. J., Ahima, R. S., Birnbaum, M. J., and Lazar, M. A. (2012) Hepatic Hdac3

promotes gluconeogenesis by repressing lipid synthesis and sequestration. *Nat. Med.* **18,** 934–942 CrossRef Medline
25. Liu, T., Zhang, L., Joo, D., and Sun, S. C. (2017) NF-κB signaling in inflammation. *Signal Transduct. Target. Ther.* **2,** 17023 CrossRef Medline
26. Chiang, J. Y. (2009) Bile acids: regulation of synthesis. *J. Lipid Res.* **50,** 1955–1966 CrossRef Medline
27. Wang, L., Han, Y., Kim, C. S., Lee, Y. K., and Moore, D. D. (2003) Resistance of SHP-null mice to bile acid-induced liver damage. *J. Biol. Chem.* **278,** 44475–44481 CrossRef Medline
28. Matsusue, K., Haluzik, M., Lambert, G., Yim, S. H., Gavrilova, O., Ward, J. M., Brewer, B., Jr., Reitman, M. L., and Gonzalez, F. J. (2003) Liver-specific disruption of PPARγ in leptin-deficient mice improves fatty liver but aggravates diabetic phenotypes. *J. Clin. Invest.* **111,** 737–747 CrossRef Medline
29. Xu, M. J., Cai, Y., Wang, H., Altamirano, J., Chang, B., Bertola, A., Odena, G., Lu, J., Tanaka, N., Matsusue, K., Matsubara, T., Mukhopadhyay, P., Kimura, S., Pacher, P., Gonzalez, F. J., *et al.* (2015) Fat-specific protein 27/CIDEC promotes development of alcoholic steatohepatitis in mice and humans. *Gastroenterology* **149,** 1030–1041.e6 CrossRef Medline
30. Matsusue, K., Kusakabe, T., Noguchi, T., Takiguchi, S., Suzuki, T., Yamano, S., and Gonzalez, F. J. (2008) Hepatic steatosis in leptin-deficient mice is promoted by the PPARγ target gene Fsp27. *Cell Metab.* **7,** 302–311 CrossRef Medline
31. Yang, C. S., Kim, J. J., Kim, T. S., Lee, P. Y., Kim, S. Y., Lee, H. M., Shin, D. M., Nguyen, L. T., Lee, M. S., Jin, H. S., Kim, K. K., Lee, C. H., Kim, M. H., Park, S. G., Kim, J. M., *et al.* (2015) Small heterodimer partner interacts with NLRP3 and negatively regulates activation of the NLRP3 inflammasome. *Nat. Commun.* **6,** 6115 CrossRef Medline
32. Yuk, J. M., Shin, D. M., Lee, H. M., Kim, J. J., Kim, S. W., Jin, H. S., Yang, C. S., Park, K. A., Chanda, D., Kim, D. K., Huang, S. M., Lee, S. K., Lee, C. H., Kim, J. M., Song, C. H., *et al.* (2011) The orphan nuclear receptor SHP acts as a negative regulator in inflammatory signaling triggered by Toll-like receptors. *Nat. Immunol.* **12,** 742–751 CrossRef Medline
33. Zhou, Z., Xu, M. J., and Gao, B. (2016) Hepatocytes: a key cell type for innate immunity. *Cell. Mol. Immunol.* **13,** 301–315 CrossRef Medline
34. Joshi-Barve, S., Barve, S. S., Amancherla, K., Gobejishvili, L., Hill, D., Cave, M., Hote, P., and McClain, C. J. (2007) Palmitic acid induces production of proinflammatory cytokine interleukin-8 from hepatocytes. *Hepatology* **46,** 823–830 CrossRef Medline
35. Ibrahim, S. H., Hirsova, P., Tomita, K., Bronk, S. F., Werneburg, N. W., Harrison, S. A., Goodfellow, V. S., Malhi, H., and Gores, G. J. (2016) Mixed lineage kinase 3 mediates release of C-X-C motif ligand 10-bearing chemotactic extracellular vesicles from lipotoxic hepatocytes. *Hepatology* **63,** 731–744 CrossRef Medline
36. Wang, W., Xu, M. J., Cai, Y., Zhou, Z., Cao, H., Mukhopadhyay, P., Pacher, P., Zheng, S., Gonzalez, F. J., and Gao, B. (2017) Inflammation is independent of steatosis in a murine model of steatohepatitis. *Hepatology* **66,** 108–123 CrossRef Medline
37. Mandrekar, P., Ambade, A., Lim, A., Szabo, G., and Catalano, D. (2011) An essential role for monocyte chemoattractant protein-1 in alcoholic liver injury: regulation of proinflammatory cytokines and hepatic steatosis in mice. *Hepatology* **54,** 2185–2197 CrossRef Medline
38. Obstfeld, A. E., Sugaru, E., Thearle, M., Francisco, A. M., Gayet, C., Ginsberg, H. N., Ables, E. V., and Ferrante, A. W., Jr. (2010) C-C chemokine receptor 2 (CCR2) regulates the hepatic recruitment of myeloid cells that promote obesity-induced hepatic steatosis. *Diabetes* **59,** 916–925 CrossRef Medline
39. Aguilar-Olivos, N. E., Carrillo-Córdova, D., Oria-Hernández, J., Sánchez-Valle, V., Ponciano-Rodríguez, G., Ramírez-Jaramillo, M., Chablé-Montero, F., Chávez-Tapia, N. C., Uribe, M., and Méndez-Sánchez, N. (2015) The nuclear receptor FXR, but not LXR, up-regulates bile acid transporter expression in non-alcoholic fatty liver disease. *Ann. Hepatol.* **14,** 487–493 CrossRef Medline
40. Ali, A. H., Carey, E. J., and Lindor, K. D. (2015) Recent advances in the development of farnesoid X receptor agonists. *Ann. Transl. Med.* **3,** 5 CrossRef Medline
41. Kim, S. C., Kim, C. K., Axe, D., Cook, A., Lee, M., Li, T., Smallwood, N., Chiang, J. Y., Hardwick, J. P., Moore, D. D., and Lee, Y. K. (2014) All-*trans*-retinoic acid ameliorates hepatic steatosis in mice by a novel transcriptional cascade. *Hepatology* **59,** 1750–1760 CrossRef Medline
42. Li, Z. Z., Berk, M., McIntyre, T. M., and Feldstein, A. E. (2009) Hepatic lipid partitioning and liver damage in nonalcoholic fatty liver disease: role of stearoyl-CoA desaturase. *J. Biol. Chem.* **284,** 5637–5644 CrossRef Medline
43. Listenberger, L. L., Han, X., Lewis, S. E., Cases, S., Farese, R. V., Jr., Ory, D. S., and Schaffer, J. E. (2003) Triglyceride accumulation protects against fatty acid-induced lipotoxicity. *Proc. Natl. Acad. Sci. U.S.A.* **100,** 3077–3082 CrossRef Medline
44. Yamaguchi, K., Yang, L., McCall, S., Huang, J., Yu, X. X., Pandey, S. K., Bhanot, S., Monia, B. P., Li, Y. X., and Diehl, A. M. (2007) Inhibiting triglyceride synthesis improves hepatic steatosis but exacerbates liver damage and fibrosis in obese mice with nonalcoholic steatohepatitis. *Hepatology* **45,** 1366–1374 CrossRef Medline
45. Renga, B., Mencarelli, A., Migliorati, M., Cipriani, S., D'Amore, C., Distrutti, E., and Fiorucci, S. (2011) SHP-dependent and -independent induction of peroxisome proliferator-activated receptor-γ by the bile acid sensor farnesoid X receptor counter-regulates the pro-inflammatory phenotype of liver myofibroblasts. *Inflamm. Res.* **60,** 577–587 CrossRef Medline
46. Rizzo, G., Disante, M., Mencarelli, A., Renga, B., Gioiello, A., Pellicciari, R., and Fiorucci, S. (2006) The farnesoid X receptor promotes adipocyte differentiation and regulates adipose cell function *in vivo*. *Mol. Pharmacol.* **70,** 1164–1173 CrossRef Medline
47. Zhang, Y., Xu, N., Xu, J., Kong, B., Copple, B., Guo, G. L., and Wang, L. (2014) E2F1 is a novel fibrogenic gene that regulates cholestatic liver fibrosis through the Egr-1/SHP/EID1 network. *Hepatology* **60,** 919–930 CrossRef Medline
48. Jung, G. S., Jeon, J. H., Choi, Y. K., Jang, S. Y., Park, S. Y., Kim, M. K., Shin, E. C., Jeong, W. I., Lee, I. K., Kang, Y. N., and Park, K. G. (2015) Small heterodimer partner attenuates profibrogenic features of hepatitis C virus-infected cells. *Liver Int.* **35,** 2233–2245 CrossRef Medline
49. Cipriani, S., Carino, A., Masullo, D., Zampella, A., Distrutti, E., and Fiorucci, S. (2017) Decoding the role of the nuclear receptor SHP in regulating hepatic stellate cells and liver fibrogenesis. *Sci. Rep.* **7,** 41055 CrossRef Medline
50. Fiorucci, S., Antonelli, E., Rizzo, G., Renga, B., Mencarelli, A., Riccardi, L., Orlandi, S., Pellicciari, R., and Morelli, A. (2004) The nuclear receptor SHP mediates inhibition of hepatic stellate cells by FXR and protects against liver fibrosis. *Gastroenterology* **127,** 1497–1512 CrossRef Medline
51. Fiorucci, S., Rizzo, G., Antonelli, E., Renga, B., Mencarelli, A., Riccardi, L., Orlandi, S., Pruzanski, M., Morelli, A., and Pellicciari, R. (2005) A farnesoid x receptor-small heterodimer partner regulatory cascade modulates tissue metalloproteinase inhibitor-1 and matrix metalloprotease expression in hepatic stellate cells and promotes resolution of liver fibrosis. *J. Pharmacol. Exp. Ther.* **314,** 584–595 CrossRef Medline
52. Sanders, K. A., Delker, D. A., Huecksteadt, T., Beck, E., Wuren, T., Chen, Y., Zhang, Y., Hazel, M. W., and Hoidal, J. R. (2019) RAGE is a critical mediator of pulmonary oxidative stress, alveolar macrophage activation and emphysema in response to cigarette smoke. *Sci. Rep.* **9,** 231 CrossRef Medline
53. Chen, E. Y., Tan, C. M., Kou, Y., Duan, Q., Wang, Z., Meirelles, G. V., Clark, N. R., and Ma'ayan, A. (2013) Enrichr: interactive and collaborative HTML5 gene list enrichment analysis tool. *BMC Bioinformatics* **14,** 128 CrossRef Medline
54. Kuleshov, M. V., Jones, M. R., Rouillard, A. D., Fernandez, N. F., Duan, Q., Wang, Z., Koplev, S., Jenkins, S. L., Jagodnik, K. M., Lachmann, A., McDermott, M. G., Monteiro, C. D., Gundersen, G. W., and Ma'ayan, A. (2016) Enrichr: a comprehensive gene set enrichment analysis web server 2016 update. *Nucleic Acids Res.* **44,** W90–W97 CrossRef Medline
55. Smalling, R. L., Delker, D. A., Zhang, Y., Nieto, N., McGuiness, M. S., Liu, S., Friedman, S. L., Hagedorn, C. H., and Wang, L. Genome-wide transcriptome analysis identifies novel gene signatures implicated in human chronic liver disease. *Am. J. Physiol. Gastrointest. Liver Physiol.* **305,** G364–G374
56. Vrochides, D., Papanikolaou, V., Pertoft, H., Antoniades, A. A., and Heldin, P. (1996) Biosynthesis and degradation of hyaluronan by nonparenchymal liver cells during liver regeneration. *Hepatology* **23,** 1650–1655 CrossRef Medline